



A spatial model of the efficiency of T cell search in the influenza-infected lung



Drew Levin ^{a,*}, Stephanie Forrest ^a, Soumya Banerjee ^a, Candice Clay ^b, Judy Cannon ^c, Melanie Moses ^a, Frederick Koster ^{a,b}

^a Department of Computer Science, University of New Mexico, Albuquerque, NM, USA

^b Lovelace Respiratory Research Institute, Albuquerque, NM, USA

^c Department of Molecular Genetics & Microbiology, Department of Pathology, University of New Mexico, Health Sciences Center, Albuquerque, NM, USA

HIGHLIGHTS

- A spatial agent-based model examines T cell search in an influenza infected lung.
- Experimental data show that chemokines CXCL10 and CCL5 are stimulated by infection.
- Rapidly expanding plaques of infection create challenges for chemotaxing T cells.
- Sensitivity analysis isolates the effects of each parameter in the model.
- Model parameters are used to determine an upper bound on T cell search time.

ARTICLE INFO

Article history:

Received 9 June 2015

Received in revised form

8 February 2016

Accepted 12 February 2016

Available online 23 February 2016

Keywords:

Agent-based model

Systems biology

Immunology

Computational biology

Virology

ABSTRACT

Emerging strains of influenza, such as avian H5N1 and 2009 pandemic H1N1, are more virulent than seasonal H1N1 influenza, yet the underlying mechanisms for these differences are not well understood. Subtle differences in how a given strain interacts with the immune system are likely a key factor in determining virulence. One aspect of the interaction is the ability of T cells to locate the foci of the infection in time to prevent uncontrolled expansion. Here, we develop an agent based spatial model to focus on T cell migration from lymph nodes through the vascular system to sites of infection. We use our model to investigate whether different strains of influenza modulate this process.

We calibrate the model using viral and chemokine secretion rates we measure in vitro together with values taken from literature. The spatial nature of the model reveals unique challenges for T cell recruitment that are not apparent in standard differential equation models. In this model comparing three influenza viruses, plaque expansion is governed primarily by the replication rate of the virus strain, and the efficiency of the T cell search-and-kill is limited by the density of infected epithelial cells in each plaque. Thus for each virus there is a different threshold of T cell search time above which recruited T cells are unable to control further expansion. Future models could use this relationship to more accurately predict control of the infection.

© 2016 Elsevier Ltd. All rights reserved.

1. Introduction

Influenza has worldwide epidemic potential with 5 million infections annually and half a million deaths ([WHO Influenza Fact Sheet, 2009](#)). Emerging strains of influenza, such as 2003 H5N1 avian and 2009 H1N1 pandemic, are more pathogenic than seasonal strains, yet the mechanisms that control this variability are not well understood. Pathogenicity is a function of both the virus

and its interaction with the immune response. Our model explores how various features of the virus and the host immune system interact to produce observed differences between strains.

Identifying the critical components of this complex process, and how they interact, is key to understanding viral pathogenicity and designing therapeutic interventions. We address this challenge through computational modeling, which allows us to study the relative contributions of different aspects of the host immune response and to account for strain-specific viral dynamics in the model. Several earlier theoretical models have been proposed to study specific aspects of influenza infections. Ordinary differential equation (ODE) models that are fit to empirical data ([Handel and](#)

* Corresponding author.

E-mail address: drew@cs.unm.edu (D. Levin).

Antia, 2008; Lee et al., 2009; Miao et al., 2010; Saenz et al., 2010; Murillo et al., 2013; Crauste et al., 2015; Price et al., 2015) have elucidated viral population level dynamics but are unable to perceive localized spatial effects. Spatial models, on the other hand, have been developed to examine interactions between dendritic cells and T cells in the lymph node (Beauchemin et al., 2005; Beltman et al., 2007; Zheng et al., 2008; Mirsky et al., 2011; Celli et al., 2012; Vroomans et al., 2012; Textor et al., 2014), but have not been extended to consider local conditions in the lung. In this paper, we examine how the unique properties of three different strains of influenza, in the presence of chemokines, affect T-cell search in the human lung.

Specifically, we focus on the interactions between activated antigen-specific CD8 T cells, cytokines, and replicating influenza virus. Chemotactic proteins are known to enhance T cell recruitment in both acute infections and chronic inflammatory diseases (Gunn et al., 1998; Medoff et al., 2005; Okada et al., 2005; Castellino et al., 2006; Bromley et al., 2008). Infected epithelial cells secrete chemokines, especially upon contact with CD8 T cells (Zhao et al., 2000; Chan et al., 2005). Previous work showed that efficient recruitment of T cells to the Focus Of Infection (FOI) is crucial for the eventual clearance of the virus (Cerwenka et al., 1999; Kim et al., 2011). As measuring real-time T cell movement in vivo lung tissue is not currently viable, study these localized processes is aided by spatial modeling of how T cells interact with the FOI and the chemotactic environment. Therefore, instead of developing a comprehensive immune system model, we present a spatially explicit agent-based model (ABM) to describe T cell interactions with chemotactic signals and a dynamically growing plaque. Using the model, we investigate the pathogenic potential of the three influenza strains: seasonal H1N1 (sH1N1), Avian H5N1 (aH5N1), and pandemic H1N1 (pH1N1). These three strains were selected for their differences in in vitro replication rates (Mitchell et al., 2011) as well as differences in in vivo severity of human and animal pneumonia and mortality.

The model is parameterized with values taken from the literature when available. Because chemokine secretion rates are central to our model and appropriate data values are not available, we estimate the parameters using data from physical experiments and our previously published ODE model (Mitchell et al., 2011).

To obtain the physical data, wells of human epithelial cells were infected with one of the three strains and then measured for virus and cytokine concentrations over a 48-hour period. Of the cytokines tested, only the chemokines CXCL10 (IP-10) and CCL5 (RANTES) were expressed differently across the three influenza strains. IP-10 and RANTES are both chemokines that normally attract T cells to the FOI (Hoji and Rinaldo, 2005; Groom and Luster, 2011a). These results suggest that the two chemokines may contribute to the immune system's varying ability to control different strains of influenza, and were thus included in our model.

The analyses of the spatial model reveal several interesting and underappreciated phenomena. The model identified physical constraints on T cells' ability to clear the rapidly replicating pH1N1 infection. Because T cells in the model use the chemokine gradient to locate the FOI, they tend to cluster in areas of high chemokine concentration. The model suggests that the chemokine response of the host cells can hinder T cells ability to find and clear infected cells in the presence of the rapidly replicating pandemic strain. A sensitivity analysis of the model parameters isolated the effects of each parameter in the model. The analysis shows that most model parameters can vary across a broad range of values without strong effect on predicted outcomes. Further analysis shows model predictions remain unchanged within broad categories of parameter type (e.g., all parameters related to chemokines, parameters related to viral kinetics, etc.). For example, the chemokine-related parameters are stable in that they do not affect the model behavior

within biologically plausible ranges. In contrast, parameters related to viral kinetics significantly alter model predictions. Finally we examine the 'window of control' which establishes an upper bound on the time it takes T cells to arrive at the FOI while still clearing the infection. We find that this value is consistent with our sensitivity analysis and helps explain the challenge of controlling the highly virulent pH1N1 strain.

2. Methods and models

2.1. Model definition

The model focuses on activated CD8 T cells migrating through the vascular and lymph networks, including their movement over tissue after extravasation (Fig. 1). While the volume of the lung consists of spherical alveoli, the spread of influenza throughout the lung occurs through the interconnected bronchiole-alveoli complex, which can be viewed as a connected monolayer. Thus, we represent the lung as a two-dimensional sheet of healthy epithelial cells (S1.3). Because we assume activated T cells descend at random into branches of the vascular network, T cells in the model are introduced uniformly at random across the modeled lung surface. If cytokine signal is detected on the local endothelium the T cell remains in tissue and follows the chemotactic gradient to the FOI. T cells that do not encounter cytokine recirculate to the lymph node where they reenter the bronchial

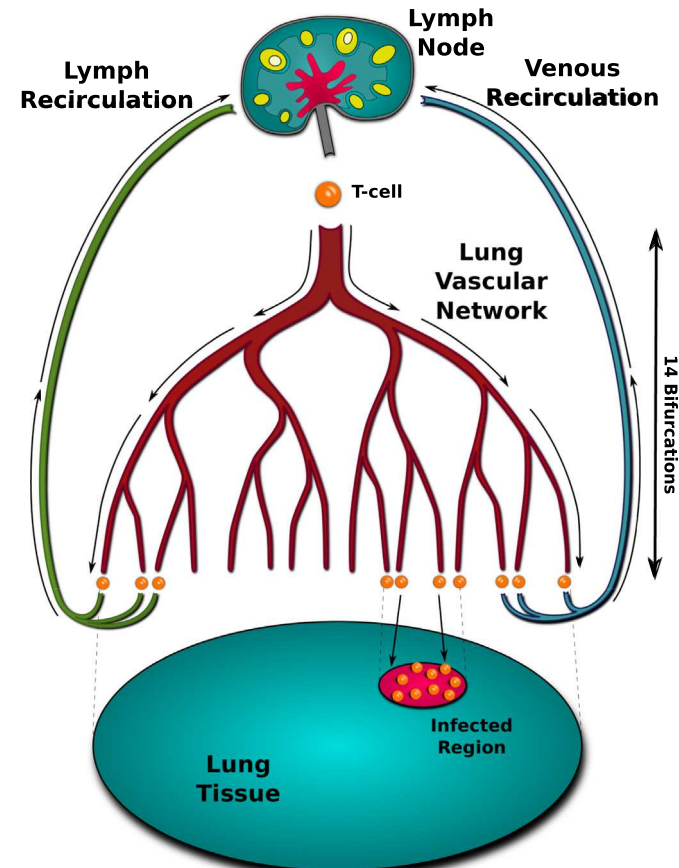


Fig. 1. Model of T cell search. Activated T cells originate in the lymph node and enter the bloodstream after which they randomly navigate through 14 vascular bifurcations of the bronchial network. Upon reaching a capillary, T cells exit into tissue if cytokine signal is present. In the absence of signal, the T cell recirculates either through the lymph network or through the pulmonary vein back to the top of the network.

vascular network. Once inside the endothelium, T cells follow the chemokine gradient to localized areas of maximum chemokine concentration. When a T cell contacts an infected epithelial cell it induces apoptosis (S1.2). Otherwise, infected cells continue to secrete virus for a fixed time and then die.

The model is initialized with a single infected cell. After the incubation period, the infected cell begins secreting virus and chemokine at rates determined by the virus strain and chemokine type (Table 1). Virus from expressing cells diffuses locally, infecting neighboring cells. Chemokine diffuses from secreting cells, creating a spreading region of stimulation around the FOI. After four simulated days, Immunoglobulin M (IgM) is introduced into the model by increasing the viral decay rate. After five simulated days, representing lymph node stimulation and T cell proliferation, activated T cells exit the lymph node at a constant rate and travel through the vasculature to the tissue as described above. These cell and molecular interactions and state transitions are depicted in Fig. 2.

2.2. Model parameters

We include only parameters that directly address the role of T cells and T cell migration because our study focuses on the role of T cells and the chemokine effects of T cells in influenza virus

infection. Thus, we included parameters that affected virus, T cells, and chemokines. With regards to the influenza, we chose parameters involving viral replication, infectivity in epithelial cells, and virus decay and diffusion rates based on our earlier study. The chemokine decay rate, diffusion rate, and secretion rate parameters are relevant to dynamic chemokine gradients required for T cell chemotaxis. Because we wanted to use our model to test the role of T cells and T cell migration in influenza clearance, we included multiple T cell parameters, such as T cell production rate, T cell death rate, T cell kill time, and T cell migration rate. We added IgM because many studies have argued for the importance of antibody mediated virus clearance. However, because our study is not addressing the role of antibody in clearance of influenza, we did not test the full range of B cell responses directly by including them in our parameters.

Model parameters are listed in Tables 1 and 2. These values were taken from the literature when available. Other parameters were determined by matching empirical data to ODE models, and some parameters were estimated using biologically plausible ranges. All estimated parameters were studied in a sensitivity analysis to test their impact on model behavior (Table 3).

Because we are interested in the interplay between the virus and the induced immune response, we infected human epithelial cells with the three different strains of influenza in vitro and measured the resulting cytokine and chemokine responses. We extended our previously published differential equation model (Mitchell et al., 2011) to obtain values for per-cell chemokine production rates. T cell production rates were derived from measured replication rates in vitro (Miao et al., 2010) using another differential equation model. T cell production is assumed to be constant after day 5 (Martin-Fontech et al., 2003).

2.3. Model implementation

The model is implemented using an updated version of the CyCells software (Warrender et al., 2006), (github.com/drewlevin/cycells), a modeling platform for two- or three-

Table 1

Strain-specific parameters. Small text values show 95% confidence intervals resulting from 1000 bootstrapping runs for each parameter (Wu and Jackknife, 1986). Bootstrapping for the chemokine values was performed using the original fit of Eq. S1 to the data in Fig. 3 to produce new data sets. Viral production values and confidence intervals are taken from Mitchell et al. (2011).

Strain	IP-10 production (pg/s · cell)	RANTES production (pg/s · cell)	Viral production (PFU/s · cell)
Avian H5N1	2.0e–4 8.4e–5–4.2e–4	1.3e–5 7.9e–6–1.9e–5	5.4e–5 4.4e–5–3.7e–4
Seasonal H1N1	1.8e–4 1.2e–4–3.0e–4	8.9e–7 4.8e–7–1.6e–6	3.8e–4 2.8e–4–1.5e–3
Pandemic H1N1	8.7e–5 1.7e–5–7.1e–4	4.3e–6 5.0e–7–3.5e–5	5.1e–3 2.8e–3–5.3e–3

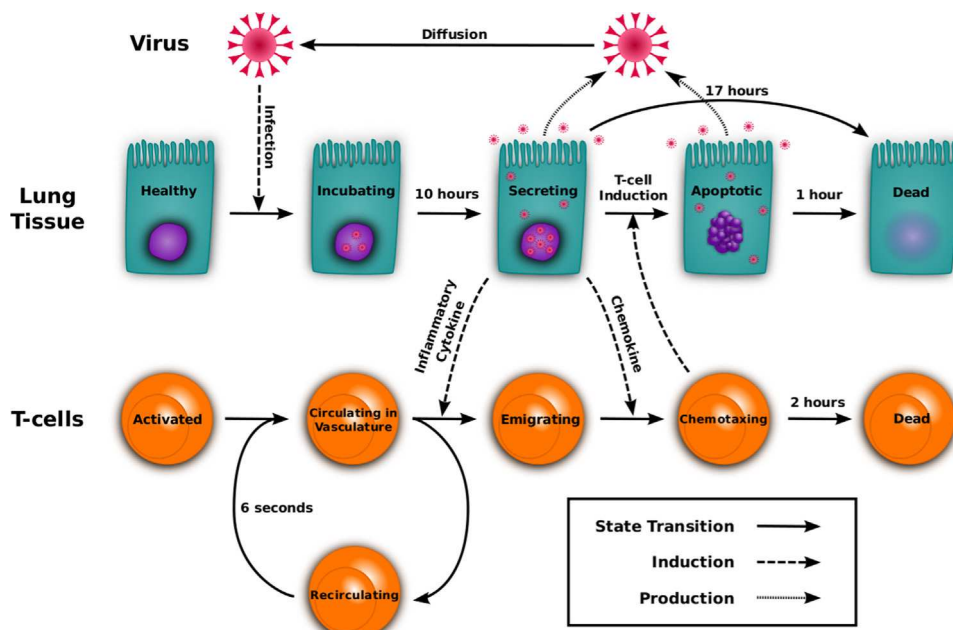


Fig. 2. Visual representation of the model. Healthy epithelial cells infected by virus begin secreting virus after the incubation delay. Activated T cells traverse the bronchial vascular network and may be recruited by inflammatory cytokine. Chemotaxing T cells climb the chemokine gradient and induce apoptosis in infected cells. Solid arrows represent a cell state transition from one behavior to another. Dashed arrows display the mechanism used to induce a transition. Dotted arrows indicate the production of new virus.

Table 2

Default values used for the model in bold. Min and max represent the extreme values tested in the sensitivity analysis (Table 3 and Figs. S3–S5).

Referenced parameters	Units	Min	Value	Max	Source
^a Viral diffusion in airway	$\mu\text{m}^2/\text{s}$	$3.18e-4$	3.18e-2	3.18	Beauchemin et al. (2006)
^a Viral decay in airway	day^{-1}	0.01	1	100	Lee et al. (2009)
Chemokine diffusion rate	$\mu\text{m}^2/\text{s}$	$3.18e-3$	0.318	318	Beauchemin et al. (2006)
Incubation time	hours	5	10	20	Mitchell et al. (2011)
Epithelial cell radius	μm	–	5	–	Elbert et al. (1999)
T Cell radius	μm	–	5	–	Abbas et al. (2011)
T Cell production rate	cells/h	125	1257	3750	Miao et al. (2010)
T Cell speed	$\mu\text{m}/\text{min}$	$6e-2$	6	600	Egen et al. (2011)
Blood circulation time	seconds	1	6	3600	Banerjee and Moses (2010)
T Cell sensitivity to chemokine	ng/mL	–	100	–	Nandagopal et al. (2011)
Onset of T Cell lymph node exit	days	–	5	–	Banerjee et al. (2011)
^a IgM viral decay factor	–	1	10	1000	Diamond et al. (2003)
IgM onset	days	–	4	–	Diamond et al. (2003)
Estimated parameters ^b	Units	Min	Value	Max	Footnote
Chemokine decay rate	Hz	$3.8e-6$	3.8e-4	$3.8e-2$	1
^a Infectivity	min/virion	12	120	1200	2
Expression time	min	100	1000	3000	Mitchell et al. (2011) ³
T Cell expected kill time	min	0	10	100	4
Apoptosis time	hours	0	1	2	Ganusov and De Boer (2008) ⁵
T Cell age (at FOI)	min	12	120	1200	6
T Cell age (in blood)	days	0.04	4	400	6

^a Denotes parameters determined to be sensitive by the one-factor-at-a-time sensitivity analysis. Values were taken from experimental literature if possible and from earlier modeling papers if not. Parameters not found in the literature were estimated as follows: (1) Corresponds to a 30 min half-life. (2) Epithelial cells are infected at a probabilistic rate such that the expected time for infection in the presence of a single virion is 2 h. This scales linearly with the number of virions in the cell's vicinity. (3) Chosen as a plausible median time (1000 min) between 6 h and 24 h. (4) T cells induce apoptosis in nearby virus-secreting epithelial cells at a probabilistic rate such that the expected time to induce apoptosis is 10 min. This rate does not scale with T cell numbers. (5) Calculated for low T cell densities. (6) Chosen to be at the lower end of biologically plausible values because increased T cell counts are shown not to affect the model behavior.

^b All estimated parameter values are examined in the sensitivity analysis (Table 3, S2.3).

Table 3

Sensitivity results: The above parameters were varied over predetermined ranges in isolation, resulting in new model runs for every new value tested (Figs. S3–S5). The results of the sensitivity analysis were then qualitatively evaluated for each individual parameter. A model run's behavior was determined by examining the height of the peak of the infection at day 5 post-infection and the number of infected cells at day 10 post-infection. Each combination of influenza strain and free parameter was classified as belonging to one of four categories. Parameters were classified as *stable* if all runs follow the same behavior, *bounded stable* if intermediate parameter adjustments did not affect the model's behavior, even if the more extreme adjustments did, *peak change* if the peak of the infection differs but the result at day 10 is the same, and *sensitive* if any level of change in the parameter affects the resulting model behavior. PRCC analysis was also performed for the H1N1 strain over these parameters (Figs. S6–S8). Bold text in the seasonal column denotes significant Spearman rank correlation ($p < 0.01$) over the time period where the parameter was active.

Category	Parameter	Avian H5N1	Seasonal H1N1	Pandemic H1N1
Chemokine	Chemokine Decay Rate	bounded stable	bounded stable	stable
	Chemokine Diffusion Rate	bounded stable	stable	stable
	Chemokine Secretion Rate	bounded stable	stable	stable
T Cell	Circulation Time	bounded stable	bounded stable	bounded stable
	T Cell Kill Rate	stable	bounded stable	bounded stable
	T Cell Speed	stable	bounded stable	bounded stable
	T Cell Age in Blood	stable	bounded stable	bounded stable
	T Cell Age at FOI	stable	bounded stable^a	bounded stable
	T Cell Production Rate	bounded stable	bounded stable	bounded stable
Delay	Apoptosis Time	stable	stable	stable
	Expression Time	peak change	peak change^a	peak change
	Incubation Time	peak change	peak change	peak change
Virus	Viral Response to IgM	sensitive	sensitive^a	sensitive
	Infectivity	sensitive	sensitive^b	sensitive
	Viral Decay Rate	sensitive	sensitive^b	sensitive
	Viral Diffusion Rate	sensitive	sensitive^b	sensitive

^aIndicates a maximum absolute Spearman's ρ of less than 0.5.

^b Indicates a maximum absolute Spearman's ρ of over than 0.5.

dimensional agent-based simulations of the immune response (S1.1). Due to computational constraints our model is scaled to the size of a mouse lung (approximately 100 cm^2), a well-established practice in spatially explicit influenza models (Miller et al., 2003; Allan et al., 2006; Ingulli et al., 2009). Parameters affected by this choice include the T cell production rate, T cell circulation time, and the total size of the lung (Table 2).

Parameters that are independent of the chosen influenza strain are shown in Table 2. Strain-specific values are shown in Table 1. Further details regarding the model definition are included in S1.2.

In the model, epithelial cells are stationary and are described by one of five sequential states: healthy, virus-incubating, virus-expressing, apoptotic, and dead (Bachem et al., 1996; Beauchemin et al., 2005; Mitchell et al., 2011). Healthy cells remain unchanged unless infected by virus. Once infected, the cell transitions from incubating to expressing after a 10 h incubation delay (Table 2). Expressing cells secrete virus and chemokine for a fixed 16.7 h and then die (Table 2). Expressing cells initiate apoptosis sooner if they are contacted by activated T cells. Apoptotic cells continue to secrete virus and chemokine and then die after one hour (Table 2). Dead cells take up space and do not regenerate over the course of an infection. Cell regrowth is not implemented as the rate of regrowth is unknown.

T cells are described by two states: circulating and chemotaxing. T cells emerge from the lymph node at five days post-infection (p.i.) at a rate of 1257 cells per hour (Models for Parameter Estimation, Table 2). T cell travel time from the lymph node to a random location on the lung's surface is six seconds. If chemokine is not encountered, the circulating T cell returns to a new location in the lung after another six seconds. If a circulating cell encounters chemokine, it changes state to chemotaxing and follows the chemotactic gradient to the FOI. Circulating T cells decay exponentially with an average lifespan of four days. Chemotaxing T cells follow the gradient through the two-dimensional lung endothelium, inducing apoptosis when they encounter expressing epithelial cells. Chemotaxing T cells decay exponentially with an average lifespan of two hours. Justifications for these parameter values are listed in Table 2.

In addition to T cells, the model contains two types of particles: virus and chemokine. Both are produced at constant rates by expressing epithelial cells. Virus diffuses through the lung tissue, infecting healthy cells at a rate proportional to the virus concentration at the location of the cell. Chemokine diffuses across the tissue but has no direct effect beyond recruiting T cells. Both particle types decay exponentially. IgM is modeled by increasing the viral decay rate by a factor of 10 after the fourth day (Table 2).

2.4. Models for parameter estimation

To provide estimates of chemokine concentrations and secretion rates in lung tissue, chemokine levels were measured at 4–6 h intervals during the first 48 h of infection in wells containing approximately one million human bronchial epithelial cells (Fig. 3, Table S1). The dynamic viral loads at these intervals have been reported previously by us for cultures infected with seasonal H1N1 virus, pandemic H1N1 virus, and avian H5N1 virus (Mitchell et al., 2011). IP-10 concentration increases were observed by 8 h post-infection (p.i.), and RANTES by 16 h p.i.

We estimate chemokine production rates, r , by adapting the delay differential equation model of influenza infection described in Mitchell et al. (2011) Eq. (1) by adding one new equation ($\dot{C} = rI_{1\tau_3} - dC$) to model chemokine production. Strain-specific values for r were found by fitting the equations to the experimental data in Table S1 using a genetic algorithm to minimize the log squared error between the model and the data while holding the rest of the parameter values constant (Fig. S1, Table S3). Next, 1000 bootstrapping runs using resampled residuals were performed on each modeled strain to generate confidence intervals over r . The results of these fits are shown in Table 1 (viral secretion rates are from previous fits in Mitchell et al., 2011). IP-10 and RANTES secretion rates are aggregated in the spatial model (S2.2):

$$\dot{T} = -\beta TV$$

$$\dot{I}_1 = \beta TV - \beta T_{\tau_1} V_{\tau_1}$$

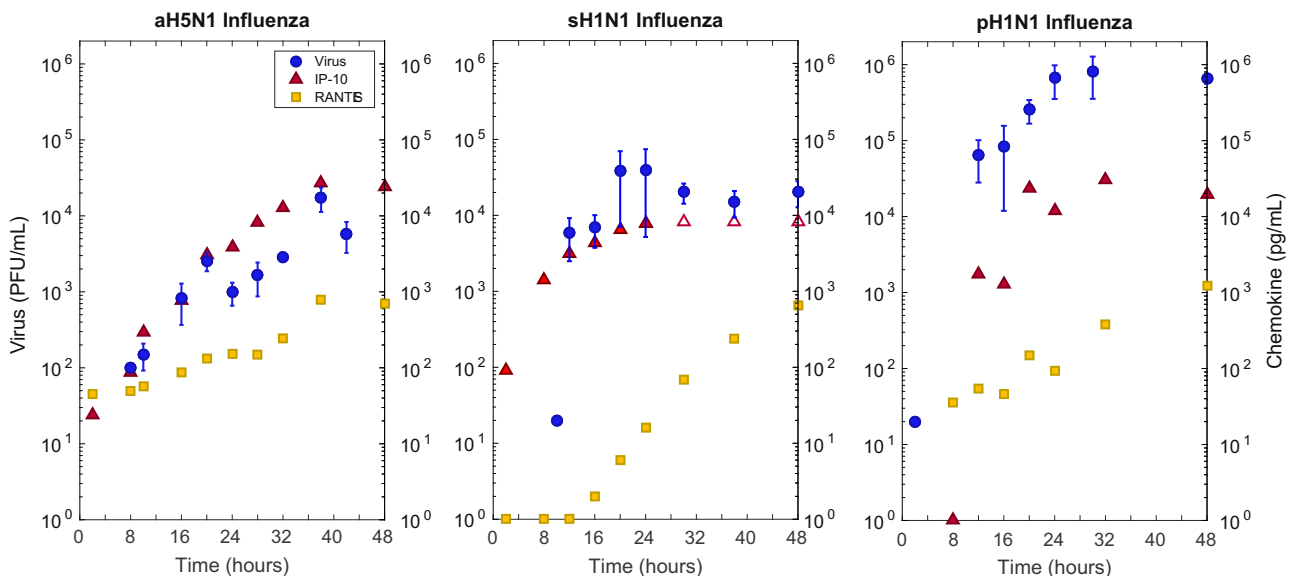


Fig. 3. Empirical viral and cytokine titers for three strains of influenza: Avian H5N1, Seasonal sh1N1, and Pandemic pH1N1. Viral titer (blue circles) is in PFU/mL, and IP-10 (red triangle) and RANTES (yellow square) are shown in pg/mL. sh1N1 IP-10 secretion exceeded measurement accuracy above 8500 pg/mL and these three values (empty red triangles) were not included in the model fitting. An extended differential equation model from Mitchell et al. (2011) was fit to IP-10 and RANTES data (Eq. (1)). These fits were used to obtain chemokine production values for use in the spatial CyCells model. Human bronchial epithelial cells were infected at an MOI of 0.01 (10,000 virions) with one of the three strains of influenza. Apical fluid for viral secretion and basal media for chemokine secretion were collected at the given time intervals post-infection. Viral culture was performed by a standard plaque assay and chemokine levels were measured using 30 μl aliquots for a panel of 17 chemokines and cytokines (not shown). (For interpretation of the references to color in this figure caption, the reader is referred to the web version of this paper.)

$$\begin{aligned} \dot{I}_2 &= \beta T_{\tau_1} V_{\tau_1} - \delta I_2 \\ \dot{V} &= \frac{p}{1+eF} I_2 - \beta TV \\ \dot{F} &= I_{1\tau_2} \\ \dot{C} &= rI_{1\tau_3} - dC \end{aligned} \quad (1)$$

τ subscript variables denote delay terms, signifying the value is the population quantity in existence at time $t - \tau$. Table S2 summarizes population and parameter values and descriptions.

We calculate the rate of production, σ , of CD8 T cells using a differential equation model from Miao et al. (2010). The equations model T cell production and subsequent search over an area of infected lung tissue:

$$\begin{aligned} N_c &= \sigma \cdot \frac{r^2 \cdot N_c}{R^2 \cdot t_{rc}} \quad \pi r^2 = a\sqrt{I} + b \\ \dot{N}'_f &= \frac{(r^2 - r') \cdot N_c}{R^2 \cdot t_{rc}} - \frac{\nu_{tcell}}{(r' - r)/2} \quad \pi r^2 = \pi r_{cell}^2 \cdot I \\ \dot{N}_f &= \frac{r^2 \cdot N_c}{R^2 \cdot t_{rc}} + \frac{\nu_{tcell}}{(r' - r)/2} \\ \dot{T} &= \rho T - \beta TV \\ \dot{I} &= \beta TV - \delta I - k_e N_f I \\ \dot{V} &= pI - \beta TV - \gamma(t)V \\ \gamma(t) &= \begin{cases} 1/\text{day} & , t < 5 \\ 3/\text{day} & , t \geq 5 \end{cases} \end{aligned} \quad (2)$$

N_c is the number of circulating activated antigen-specific CD8 T cells, N'_f is the number of circulating T cells that have found and exit into a region of lung tissue expressing chemokines, N_f is the number of circulating T cells that have found an infected region. T is the number of uninfected target cells, I is the number of productively infected cells, and V is the viral titer in serum. The infected region is assumed to be of radius r and is within a region expressing chemokines of radius r' ($r < r'$). The lung is modeled as a circular region with radius R . The area of the infected region is equal to the area of an infected cell (of radius r_{cell}) multiplied by the number of infected cells. See Fig. 1 for more details about the model. The area of the region expressing chemokine was found to be related non-linearly to the number of infected cells ($\pi r^2 = a\sqrt{I} + b$) where a and b are constants that depend on the viral strain. a and b were fit to 5 experimental runs of a spatial model implemented in CyCells ($R^2 = 0.997$, $P < 0.01$).

Circulating CD8 T cells (N_c) are assumed to be released from lymph nodes at a constant rate σ and circulate to the N'_f population over a time defined by t_{rc} . We assume these circulating cells transition into N'_f and N_f at rates proportional to the areas of the chemokine expressing and infected regions relative to the whole lung area.

The average time an exiting CD8 T cell takes to migrate to the infected region is equal to the difference in the radii between the two regions ($r' - r$) times the T cell speed, ν_{tcell} . Circulating cells that are in the chemokine expressing region (N'_f) move into the infected region after performing chemotaxis for that time. Target cells (T) become infected by virus at rate βTV , where β is the rate constant characterizing infection. Infected cells (I) die at rate δ in addition to being lysed by T cells (N_f) at a rate k_e . Finally the viral titers (V) increase due to production of virus at rate p by infected cells. Virus is also cleared due to uptake by infected cells (at a rate $-\beta TV$) and due to antibody (at a rate $\gamma(t)$ that changes after 5 days post-infection). The initial viral titer was initialized to 10,000 PFUs and the initial number of target cells was one million. The initial number of infected cells is assumed to be zero. Parameter values are listed in Table S4. This ODE was fit to data taken from Miao et al. (2010) using Matlab's `nlinfit` function in order to obtain a value for σ . The final value was found to be 1257 per hour.

2.5. Materials

In an effort to obtain per-cell chemokine and cytokine production rates, human epithelial cells were infected with influenza in vitro. Epithelial cell culture and supernatant collection was performed as described in Mitchell et al. (2011). Briefly, undifferentiated human tracheal epithelial cells (University of Miami) were cultured for 4 weeks to achieve fully differentiated confluent monolayers on collagen-coated transwell inserts, or commercial differentiated human bronchial epithelial cells (EpiAirway Tissue, MatTek Corp., Ashland, MA) used immediately upon receipt were infected at an MOI of 0.01 with either seasonal H1N1 virus A/New Caledonia/20/99 (sH1N1), the 2009 H1N1 pandemic strain A/California/04/09 (pH1N1), or avian H5N1 virus A/Hong Kong/483/97 (aH5N1) derived from a fatal human infection. Basal media was collected from previously undisturbed triplicate or quadruplicate wells at 0, 6, 10, 12, 16, 20, 24, 30, 36, 42, 48, and 72 h after infection, and stored at -80°C until assay. Subsequently, apical fluid for virus secretion was collected before and after treatment of the monolayer with protease (Pronase, Sigma) to optimize the collection of infectious virus (Mitchell et al., 2011). Quantitative viral culture was performed by standard plaque assay. Quantitative chemokine levels were performed in 30 μL aliquots for a panel of chemokines (IL-8, MCP-1, MIP-1 α , MIP-1 β , RANTES, IP-10, eotaxin) and cytokines (interferon-gamma, IL-1 α , IL-1 β , IL-1RA, IL-2, IL-3, IL-4, IL-6, IL-10, IL-12p40, IL-15, IL-17, TNF α) (Luminex Assay, Luminex Corp.) and reported as ng/mL basal media sampled from a total volume of 4 mL. Only IP-10, RANTES, and TNF α showed increases in production (Table S1). TNF activity is not incorporated in the model. Data for other chemokines and cytokines is not shown.

3. Results

3.1. Model results

Because the CyCells model is stochastic, we conducted 100 runs of the model with the same parameter set for each of the three influenza strains, each run initialized with a unique random seed (Fig. 4). We count the number of infected cells in the simulated plaque at every time point. For the avian and seasonal strains, all model runs cleared the infection by day 10. Conversely, each simulation of the 2009 pandemic influenza led to uncontrolled infection.

We estimated variance across runs by calculating the standard deviation at each time point. For aH5N1, the maximum standard deviation was 35, which occurred at day 4.8 where the mean value was 257. For sH1N1, the maximum standard deviation was 212, which occurred at day 5.1 where the mean value was 2528. For pH1N1, the maximum standard deviation was 231, which occurred at day 5.1 where the mean value was 6988 (Fig. 4).

In all studied strains, virus population growth slows at four days p.i. (Fig. 4), due to IgM appearance. Subsequently, the simulated CD8 T cell response causes the number of infected cells to decline quickly after day five p.i. aH5N1 is cleared completely, sH1N1 is cleared more slowly. In contrast, at day six p.i., pH1N1 replication overwhelms the IgM and T cell response. These results are consistent with previously reported in vitro differences among the three different strains (Mitchell et al., 2011).

3.2. Spatial effects

Plaque growth in the model is illustrated in Fig. 5 and Videos S1–S3. Because the virus particles are an order of magnitude larger than the chemokine molecules, they diffuse more slowly according

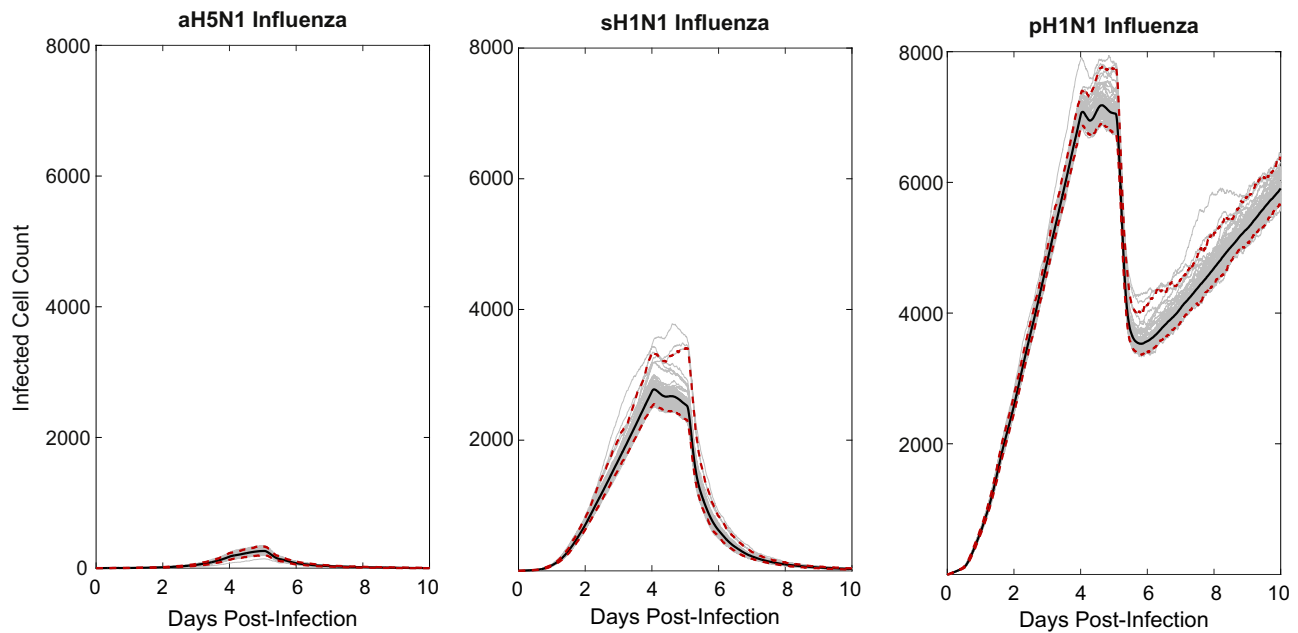


Fig. 4. Model results: Time series plots of 100 runs of aH5N1 (A), sH1N1 (B), and pH1N1 (C) infections (gray). Each run took the calculated viral production and chemokine production rates for the three different strains of influenza as input (Table 1) and reported the total number of infected cells, including incubating, virus secreting and apoptotic, but not including dead cells. Therefore the figures approximate the rate of plaque growth over time. IP-10 and RANTES were simulated in each run, except for aH5N1, which produced only RANTES. Each run was initialized identically for each strain save for the random seed. The middle line shows the mean while the red dashed lines show the 96% credible confidence interval. (For interpretation of the references to color in this figure caption, the reader is referred to the web version of this paper.)

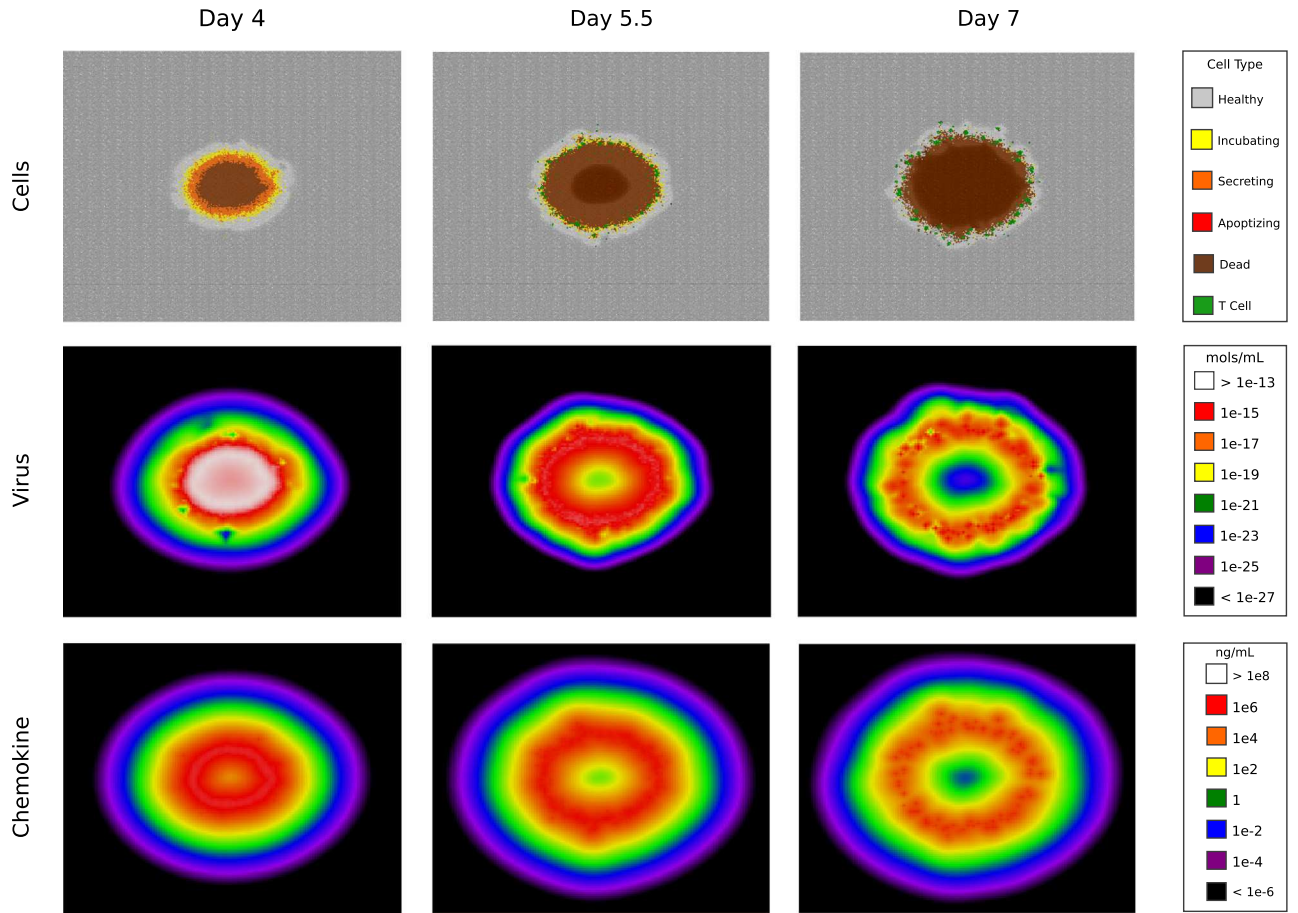


Fig. 5. Simulated sH1N1 infection. Screenshots from day 4, day 5.5, and day 7. The top row shows the spreading focus of infection through the color coding of individual cells: healthy cells in uninfected tissue (gray), virus-incubating cells (yellow), virus-secreting cells (orange), apoptotic cells (red), dead cells (brown), and T cells arriving at day 5 (green). Free virus and chemokine particles are represented by compartmentalized concentrations of mols/mL and ng/mL. Chemokine shown is an aggregate of total IP-10 and RANTES concentrations. See Videos S1–S3 for an animated visualization of each row. (For interpretation of the references to color in this figure caption, the reader is referred to the web version of this paper.)

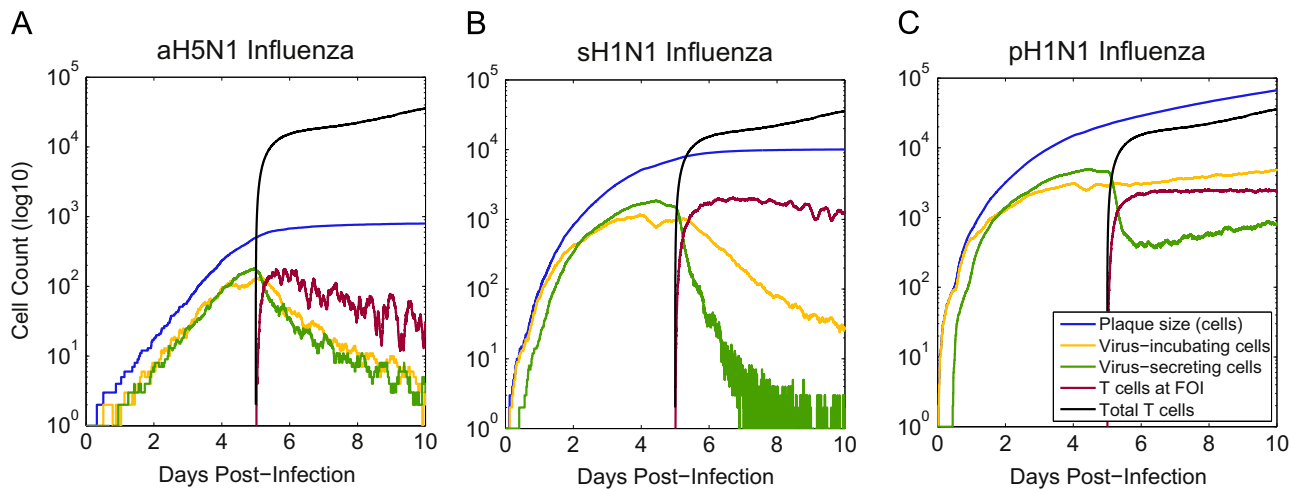


Fig. 6. Simulated infections of aH5N1, sH1N1, and pH1N1. Plotted values: total plaque size (blue), number of virus incubating cells (yellow), number of virus secreting cells (green), total number of T cells (black), and T cells at the focus of infection (FOI) (red). T cells clear secreting and incubating cells in aH5N1, fail to clear incubating cells in sH1N1, and fail to clear either type of infected cell in pH1N1. The number of incubating cells (yellow) after day 5 differs markedly among the three strains indicating that the T cells have differing success at controlling the infection. (For interpretation of the references to color in this figure caption, the reader is referred to the web version of this paper.)

to the Stokes–Einstein equation. However, chemokine molecules decay more quickly than the virus (Table 2). In the model these countervailing characteristics produce similar spatio-temporal profiles for the two particle types (Fig. 5). Before day 4 the plaque is populated primarily by virus-incubating and virus-secreting cells, with a small percentage of dead cells (Panel A). Over time, cells in the plaque's interior die, and active cells comprise a decreasing proportion of the plaque. T cells arrive at day 5 and begin killing the virus-secreting cells (Panel B). By day 6 many expressing cells have been eliminated and the plaque is populated by dead cells (Panel C).

Supplementary data associated with this article can be found in the online version at <http://dx.doi.org/10.1016/j.jtbi.2016.02.022>.

In the aH5N1 infection, the plaque is densely populated with infected cells, allowing T cells to find secreting cells easily and clear the infection (Fig. 6A). However, secreting cells were not cleared in either the sH1N1 or pH1N1 simulations (Fig. 4). In these runs, virus-secreting cells accounted for at most 10% of the active cell population and less than 1% of the total plaque at 6 days p.i. (Fig. 6). T cells continue to accumulate, but they arrive at a slower rate than the rate at which new cells become infected. Further, the newly arriving T cells are less efficient because the infected epithelial cells are more sparsely distributed in the plaque.

Finally, the spatial nature of our model reveals that the locations of peak chemokine concentration can move more slowly than the rate infected cells and virus expand, thus misdirecting the T cells. It takes time for infected cells to begin producing chemokine, while the preexisting areas of high chemokine density are slow to decay. Thus, T cells whose movements respond to the spatial layout of the chemokine gradient can become trapped, failing to locate new regions of infected cells in the growing plaque. The differences in the infection outcomes between the three strains illustrate the effect of the infection spreading faster than the chemokine maxima can move in the case of pH1N1. The velocity of the chemokine maxima positions depends on a combination of many factors, including the chemokine diffusion, decay, delay, and secretion rates (Table 2).

3.3. Sensitivity analysis

We performed two sensitivity analyses of 16 model parameters to identify those that have an effect on determining model

outcomes (S2.3–S2.4). We studied all but five of the parameters listed in Tables 1 and 2, excluding T cell radius, T cell sensitivity to chemokine, T cell onset time, IgM onset time, and the viral production rate. T cell radius is known (Abbas et al., 2011) and does not factor strongly into the spatial model's implementation. T cell sensitivity was set to mimic a realistic threshold of response to cytokine (see S2.1 for a more complete explanation of how T cell sensitivity was determined). The two onset parameters are known (Diamond et al., 2003). Viral production is an independent variable, as discussed above, and determined by each of the three strains (Mitchell et al., 2011).

Each of the remaining 16 parameters was varied independently (over multiple orders of magnitude when appropriate) for each viral strain using a one-factor-at-a-time (OFAT) approach, and the model was rerun once for each parameter setting (S2.3). Results were compared for the quantitative size of the peak infection and the number of uncleared infected cells at day 10 p.i. Based on these runs, we classified each parameter for each strain as follows (Table 3): *stable* parameters are those that do not affect the model behavior over any of the different values tested; *bounded stable* parameters are stable across a biologically plausible range of values but model behavior diverges at some threshold; *peak change* parameters affect the peak size of the infection, but do not change the ultimate number of infected cells at the end of the run; and *sensitive* parameters substantively change the outcome of the simulation within biologically plausible ranges.

Table 3 shows that four parameters are sensitive: viral response to IgM, infectivity, viral decay rate, and viral diffusion. In addition, Fig. 4 shows that viral production rate is a sensitive parameter, varying among the three panels. The four parameters (infectivity, viral decay rate, viral diffusion rate, and viral production rate) are specific viral characteristics. Further, viral response to IgM, as coded in the model, directly affects viral decay rate and can be considered a viral parameter. None of the T cell parameters nor the chemokine parameters has a strong effect on the model's prediction of control or lack of control of viral replication. This result supports the hypothesis that virus dynamics dominate the course of an influenza infection.

Partial rank correlation coefficient (PRCC) analysis was performed on the sH1N1 strain as described in Marino et al. (2008) using the same 16 parameters plus the viral secretion rate to determine the strength and significance of the parameters' partial

correlation with the model output (S2.4). The five viral parameters are confirmed by the PRCC analysis to be significantly correlated with model output (Table 3). Consistent results between the two approaches suggests the less computationally intensive OFAT analysis is also accurate for aH5N1 and pH1N1.

3.4. Window of control

Our sensitivity analysis suggests that viral parameters are the most sensitive and have the largest effect on the course of the infection (Table 3). Here we examine the role of T cells by assessing multiple factors that control the overall T cell response. We seek to identify the maximum amount of time virus-secreting cells may produce virus while still allowing the infection to be cleared. We name this threshold the ‘window of control’. This window can be defined as the combination of the time of T cell arrival at a virus-secreting cell (T_{arr}), the time it takes for the T cell to induce apoptosis (T_{kill}) and the time for the infected cell to apoptose (T_{apop}). We examine how much virus a virus-secreting cell can produce inside this window. Values above one suggest a growing infection, while values below one suggest infection control.

An epithelial cell infected with pH1N1 produces new virus at the rate of $5.1e-3$ PFU/s (Table 1). Assuming instantaneous T cell arrival at a new virus-secreting cell, T cell-induced apoptosis occurs within 10 min (T_{kill}) and viral secretion continues for 60 min after that (T_{apop}) according to our model (Table 2). Under these circumstances the cell produces 21 new viral particles that can infect new cells in this 70 min window that occurs after T cell arrival. In contrast, with the sH1N1 strain, a single infected cell produces 1.6 viral particles, and for the aH5N1 strain this number is 0.2.

Even if T cell arrival and apoptosis time were instantaneous, a cell would still secrete virus for 10 min (T_{kill}), producing 3 new virions in the case of pH1N1. Only in the case where both T_{kill} and T_{apop} are simultaneously reduced can the pandemic infection be limited to less than one new virion per infected cell. We confirm this effect in the model by first setting both relevant parameters (apoptosis time and T cell kill time) to zero, and as expected all three strains were cleared (Fig. 7). We now ask how much T cell arrival delay the model can tolerate and still clear a given viral strain. To answer this, we formulate the basic equations of the model in terms of R_0 , the viral replication rate, and solve for the case where $R_0 < 1$:

$$R_0 = p \times (T_{arr} + T_{kill} + T_{apop}) \times E \quad (3)$$

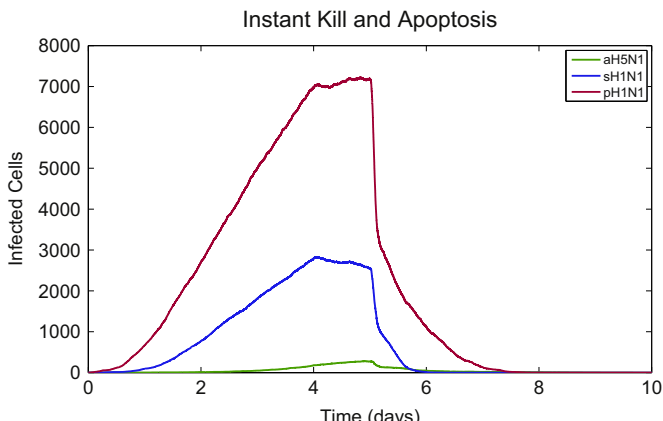


Fig. 7. Simulated infections of aH5N1, sH1N1, and pH1N1 with instant cell death. The model results show that the combined delay of the T cell kill time and apoptosis time form a barrier to infection clearance. Removing both delays results in infection clearance for all strains.

where p is the secretion rate of the virus and E is viral effectiveness, i.e. the proportion of virus that infects cells. Eq. (1) assumes each free virus particle can infect no more than one healthy epithelial cell.

p , T_{kill} , and T_{apop} are model parameters (Table 2). E incorporates both spatial effects of viral diffusion and temporal effects of viral decay. As the infected plaque expands, some secreted virus diffuses to cells that are already infected or dead (the existing plaque) and do not contribute to new infections. This effect is minimal in the beginning when the edge of the plaque is small and tightly curved. As the plaque expands, its radius grows and the edge approaches the limiting case of a straight line when 50% of the virus could be expected to diffuse over healthy cells and 50% over infected or dead cells. In the presence of healthy cells, virions infect the cells at a rate of 0.5/h and decay at a rate of 0.42/h in the presence of IgM after day 4 p.i. (Table 2). This suggests that 50% of free virus contacts healthy cells and 54% of that virus succeeds in infecting a healthy cell, implying that $E \approx 0.27$ (see S2.5 for a more complete explanation of how E was determined). Solving for T_{arr} where $R_0 < 1$ gives:

$$\lim_{t \rightarrow \infty} T_{arr} < \frac{1}{pE} - (T_{kill} + T_{apop}) \quad (4)$$

Using the model parameters, this equation suggests that $T_{arr} < 18$ h for aH5N1 and $T_{arr} < 93$ min for sH1N1. pH1N1, however, cannot be cleared for any value of T_{arr} in this scenario.

The above calculation suggests a combined transition point for sH1N1 at 163 min ($R_0 = 1$ for $T_{arr} + T_{kill} + T_{apop} = 163$ min), which is consistent with the sensitivity analysis (Fig. S5: Apoptosis Time: 90–120 min) and suggests that the modeled T_{arr} is between 33 and 63 min for sH1N1. These data show that the balance between viral production and T cell response is a key factor in clearance of infection: pH1N1 can theoretically be cleared with instantaneous T cell effectiveness (Fig. 7), but in actuality viral production exceeds T cell response time and this leads to uncontrolled infection.

4. Discussion

We used a spatial model to study how T cell search in the lung affects the host's ability to clear virus. CD8 T cells conduct two ‘searches’ in two different tissue environments, first to encounter antigen-loaded dendritic cells in the lymph node, and second to encounter local inflammatory signals in the infected lung. Search problems in the lymph node have been simulated using live cell imaging data to provide reliable parameters of cell movement (Mirsky et al., 2011; Vroomans et al., 2012). Our model focused on the second search, i.e. the process of recruiting activated CD8 effector cells to infected sites in the lung, which is not as well understood. In contrast to the dense 3D lymph node volume, our model approximates a mouse lung as a 2D surface where the epithelial cell monolayer is 100 cm^2 (only the area containing the FOI is modeled explicitly). T cells must somehow rapidly locate the infection, which at day 5 p.i. is approximately 0.5 mm in diameter. Our model revealed four main insights regarding chemokine aided T cell search in the lung.

First, the model consistently clears the aH5N1 strain by day 10 p.i., contains sH1N1 by day 10 p.i., and fails to clear the pH1N1 infection. Second, the model revealed spatial constraints on T cell search when the infection spreads more quickly than the chemokine gradient can diffuse. In these cases, T cells become trapped in areas of high chemokine concentration which lag behind the expanding infection. High concentrations of chemokine also attract and trap arriving T cells, thus limiting the direct benefit of increasing numbers of T cells. Third, the sensitivity analysis tested the individual effects of each parameter on the model's behavior.

The analysis shows that infection outcomes are highly sensitive to the properties of the specific virus. Finally, we examined the window of control which suggests that pandemic influenza could not be cleared even if T cell arrival was instantaneous.

The in vivo quantitative chemokine parameters in the infected lung are difficult to estimate. There is clear evidence from multiple models that chemokines and chemokine receptors are required for effector T cell localization to infected tissues (Christensen et al., 2004, 2006; Dawson et al., 2000; De Lemos et al., 2005; Fadel et al., 2008; Gadhamsetty et al., 2014; Groom and Luster, 2011a, 2011b; Hsieh et al., 2006; Klein et al., 2005; Kohlmeier et al., 2009, 2011; Thapa et al., 2008; Wareing et al., 2004; Wuest and Carr, 2008; Pawelek et al., 2012). However, the actual effect of chemokines on effector T cells in tissues is still largely unknown. Blood levels documented in virulent influenza infections (De Jong et al., 2006) may not reflect lung tissue concentrations. Dynamic chemokine concentrations secreted by bronchial epithelial cells in vitro depend on infection intensity and cell maturation state (Mitchell et al., 2011; Chan et al., 2010, 2005; Zeng et al., 2011) and may better approximate chemokine levels in tissue. We have determined the level of chemokine released by infected bronchial epithelial cells (Table 1) and used these as the best approximation for chemokine levels in tissues. Our model did not incorporate the potential contributions from other cytokines that did not show different levels in the physical experiment. This includes chemokines such as CXCL8/IL-8 detected in bronchial cell cultures (Matsukura et al., 1996; Arndt et al., 2002) as well as chemokines secreted by immigrant macrophages (Julkunen et al., 2000), neutrophils (Lim et al., 2015), and amplification of epithelial cell secretion by CD8 T cells (Zhao et al., 2000). The sensitivity analysis classifies the chemokine secretion rate as stable, suggesting the total amount of chemokine is not a significant factor in determining viral clearance in our model.

Although leukocytes exhibit directional behavior to chemokines (Li Jeon et al., 2002; McDonald et al., 2010), CD8 T cells have not yet been shown to climb chemokine gradients. While T cell chemotaxis may not be proven, our previous work suggests severe limitations to viral clearance in the absence of this ability (Banerjee et al., 2011). Our sensitivity analysis shows that slowing T cell speed (and consequently, the ability of T cells to climb gradients) reduces clearance of sH1N1 and pH1N1 strains. These results are consistent with the hypothesis that T cells are guided by chemokine in the lung epithelium.

Previous ODE models have studied how viral dynamics affect the course of infection (Handel and Antia, 2008; Lee et al., 2009; Miao et al., 2010; Mitchell et al., 2011; Saenz et al., 2010; Crauste et al., 2015; Price et al., 2015). The use of an ABM can complement spatially homogeneous differential equation models (Beltman et al., 2007; Textor et al., 2014; Vroomans et al., 2012; Zheng et al., 2008). In this study, we tested how chemokine-directed T cell search contributes to infection clearance. Explicitly modeling T cell chemotaxis revealed unique challenges to viral clearance brought about by infections that spread more rapidly than the chemokine gradient could decay and diffuse. Furthermore, our model was also able to account for spatial constraints of viral diffusion and infection. Fig. 5 illustrates how new virus diffuses over cells that are no longer able to be infected. ODE models account for this discrepancy by lowering rates of infection by a constant amount, but this assumes that the proportion of unsuitable virions will always be the same. Our model visualizes how the early infection has a higher proportion of virus overlapping healthy cells (Fig. 5).

In our spatial model, CD8 T cells climb a chemokine gradient to find infected epithelial cells and cluster at local maxima of chemokine concentration. Because T cells are clustered, they cannot cover the expanding plaque effectively, where infected cells on the periphery become more highly dispersed as the plaque grows.

Thus, T cells in the model become redundant at a relatively low threshold, beyond which additional T cells do not improve clearance rates. These observations provide an explanation for pH1N1 dynamics that would be obscured without the visualizations provided by spatial modeling.

The window of control describes the limit on the amount of time an infected cell may secrete virus while still allowing the infection to be cleared. Studying the time of T cell arrival at virus-secreting cells in the model revealed one reason why T cells fail to clear pH1N1 infections. We formalized this effect in an equation which calculates an upper bound on the search time for T cells to find new virus-secreting cells, and we showed that this value is consistent with the results of our sensitivity analysis.

Our model captures important quantitative and spatial aspects of T cell response to influenza infection which have not been addressed by earlier T cell models. The results of our sensitivity analysis are important for future biological modeling and experimental design. Empirical verification of the model's sensitive parameters (viral response to IgM, infectivity, viral decay rate, viral diffusion rate, and viral production rate) will be valuable to future studies. Finally, knowledge of the spatial nature of the interaction between T cells and chemokines can aid in the design of future immune system models.

Acknowledgments

We thank F. Aspert-Boursin (UNM Pathology and Computer Science), S. Jordan (UNM Computer Science and Biology), and G. Bezerra, B. Edwards, ThanhVu Nguyen, and G. Stelle (UNM Computer Science) for suggestions concerning the manuscript, cellular and chemokine behavior, and agent-based modeling.

This publication was funded by NIH Grants 1R21-AI-73607 (to F.K.), U01-AI-074561 (to F.K.), DARPA Grant P-1070-113237 (to S.F.), and NSF Grant EF 1038682 (to M.M.) and a James S. McDonnell Foundation Complex Systems Scholar Award (to M.M.).

Appendix A. Supplementary data

Supplementary data associated with this article can be found in the online version at <http://dx.doi.org/10.1016/j.jtbi.2016.02.022>.

References

- Abbas, A.K., Lichtman, A.H.H., Pillai, S., 2011. *Cellular and Molecular Immunology*. Saunders.
- Allan, R.S., Waithman, J., Bedoui, S., Jones, C.M., Villadangos, J.A., Zhan, Y., Lew, A.M., Shortman, K., Heath, W.R., Carbone, F.R., 2006. Migratory dendritic cells transfer antigen to a lymph node-resident dendritic cell population for efficient CTL priming. *Immunity* 25 (1), 153–162, URL <http://www.ncbi.nlm.nih.gov/pubmed/16860764>.
- Arndt, U., Wennemuth, G., Barth, P., Nain, M., Al-Abed, Y., Meinhardt, A., Gemsa, D., Bacher, M., 2002. Release of macrophage migration inhibitory factor and CXCL8/interleukin-8 from lung epithelial cells rendered necrotic by influenza A virus infection. *J. Virol.* 76 (18), 9298–9306, URL <http://view.ncbi.nlm.nih.gov/pubmed/12186913>.
- Bachem, A., Hochstättler, W., Malich, M., 1996. The simulated trading heuristic for solving vehicle routing problems. *Discret. Appl. Math.* 65 (1), 47–72.
- Banerjee, S., Moses, M., 2010. Scale invariance of immune system response rates and times: perspectives on immune system architecture and implications for artificial immune systems. *Swarm Intell.* 4 (4), 301–318. <http://dx.doi.org/10.1007/s11721-010-0048-2>, ISSN 1935-3812, URL <http://www.springerlink.com/index/10.1007/s11721-010-0048-2>.
- Banerjee, S., Levin, D., Moses, M., Koster, F., Forrest, S., 2011. The value of inflammatory signals in adaptive immune responses. *ICARIS* 6825, 1–14.
- Beauchemin, C., Samuel, J., Tuszyński, J., 2005. A simple cellular automaton model for influenza A viral infections. *J. Theor. Biol.* 232 (2), 223–234.

- Beauchemin, C., Forrest, S., Koster, F.T., 2006. Modeling influenza viral dynamics in tissue. *LNCS Artif. Immune Syst.* 4163, 23–36, ISSN 03029743, URL <http://www.springerlink.com/content/9754174j200113jv/>.
- Beltman, J.B., Marée, A.F.M., De Boer, R.J., 2007. Spatial modelling of brief and long interactions between T cells and dendritic cells. *Immunol. Cell Biol.* 85 (4), 306–314, URL <http://www.ncbi.nlm.nih.gov/pubmed/17420768>.
- Bromley, S.K., Mempel, T.R., Luster, A.D., 2008. Orchestrating the orchestrators: chemokines in control of T cell traffic. *Nat. Immunol.* 9 (9), 970–980. <http://dx.doi.org/10.1038/nifi.213>, ISSN 1529-2916, URL <http://www.ncbi.nlm.nih.gov/pubmed/18711434>.
- Castellino, F., Huang, A.Y., Altan-Bonnet, G., Stoll, S., Scheinecker, C., Germain, R.N., 2006. Chemokines enhance immunity by guiding naive CD8+ T cells to sites of CD4+ T cell-dendritic cell interaction. *Nature* 440 (7086), 890–895. <http://dx.doi.org/10.1038/nature04651>, ISSN 14764687, URL <http://www.ncbi.nlm.nih.gov/pubmed/16612374>.
- Celli, S., Day, M., Müller, A.J., Molina-Paris, C., Lythe, G., Bousso, P., 2012. How many dendritic cells are required to initiate a T-cell response? *Blood* 120, 3945–3948. <http://dx.doi.org/10.1182/blood-2012-01-408260>, ISSN 00064971.
- Cerwenka, A., Morgan, T.M., Harmsen, A.G., Dutton, R.W., 1999. Migration kinetics and final destination of Type 1 and Type 2 CD8 effector cells predict protection against pulmonary virus infection. *J. Exp. Med.* 189 (2), 423–434, URL <http://www.ncbi.nlm.nih.gov/articlerender.fcgi?artid=2192982&tool=pmcentrez&rendertype=abstract>.
- Chan, M.C.W., Cheung, C.Y., Chui, W.H., Tsao, S.W., Nicholls, J.M., Chan, Y.O., Chan, R.W.Y., Long, H.T., Poon, L.L.M., Guan, Y., Peiris, J.S.M., 2005. Proinflammatory cytokine responses induced by influenza A (H5N1) viruses in primary human alveolar and bronchial epithelial cells. *Respir. Res.* 6 (1), 135, URL <http://www.ncbi.nlm.nih.gov/pubmed/16283933>.
- Chan, R.W.Y., Yuen, K.M., Yu, W.C.L., Ho, C.C.C., Nicholls, J.M., Peiris, J.S.M., Chan, M.C.W., 2010. Influenza H5N1 and H1N1 virus replication and innate immune responses in bronchial epithelial cells are influenced by the state of differentiation. *PLoS ONE* 5 (1), 9, URL <http://www.ncbi.nlm.nih.gov/articlerender.fcgi?artid=2806912&tool=pmcentrez&rendertype=abstract>.
- Christensen, J.E., Nansen, A., Moos, T., Lu, B., Gerard, C., Christensen, J.P., Thomsen, A.R., 2004. Efficient T-cell surveillance of the CNS requires expression of the CXC chemokine receptor 3. *J. Neurosci.* 24 (20), 4849–4858, URL <http://www.ncbi.nlm.nih.gov/pubmed/15152045>.
- Christensen, J.E., De Lemos, C., Moos, T., Christensen, J.P., Thomsen, A.R., 2006. CXCL10 is the key ligand for CXCR3 on CD8+ effector T cells involved in immune surveillance of the lymphocytic choriomeningitis virus-infected central nervous system. *J. Immunol.* 176 (7), 4235–4243, URL http://www.ncbi.nlm.nih.gov/entrez/query.fcgi?cmd=Retrieve&db=PubMed&dopt=Citation&list_uids=16547260.
- Crauste, F., Terry, E., Mercier, I.L., Mafile, J., Djebali, S., Andrieu, T., Mercier, B., Kaneko, G., Arpin, C., Marvel, J., Gandrillon, O., 2015. Predicting pathogen-specific CD8 T cell immune responses from a modeling approach. *J. Theor. Biol.* 374, 66–82. <http://dx.doi.org/10.1016/j.jtbi.2015.03.033>, ISSN 00225193, URL <http://www.sciencedirect.com/science/article/pii/S0022519315001484>.
- Dawson, T.C., Beck, M.A., Kuziel, W.A., Henderson, F., Maeda, N., 2000. Contrasting effects of CCR5 and CCR2 deficiency in the pulmonary inflammatory response to influenza A virus. *Am. J. Pathol.* 156 (6), 1951–1959. [http://dx.doi.org/10.1016/S0002-9440\(10\)65068-7](http://dx.doi.org/10.1016/S0002-9440(10)65068-7), ISSN 0002-9440, URL <http://www.ncbi.nlm.nih.gov/articlerender.fcgi?artid=1850091&tool=pmcentrez&rendertype=abstract>.
- De Jong, M.D., Simmons, C.P., Thanh, T.T., Hien, V.M., Smith, G.J.D., Chau, T.N.B., Hoang, D.M., Chau, N.V. V., Khanh, T.H., Dong, V.C., Qui, P.T., Cam, B.V., Ha, D.Q., Guan, Y., Peiris, J.S.M., Chinh, N.T., Hien, T.T., Farrar, J., 2006. Fatal outcome of human influenza A (H5N1) is associated with high viral load and hypercytopenia. *Nat. Med.* 12 (10), 1203–1207, URL <http://www.ncbi.nlm.nih.gov/pubmed/16964257>.
- De Lemos, C., Christensen, J.E., Nansen, A., Moos, T., Lu, B., Gerard, C., Christensen, J.P., Thomsen, A.R., 2005. Opposing effects of CXCR3 and CCR5 deficiency on CD8+ T cell-mediated inflammation in the central nervous system of virus-infected mice. *J. Immunol.* 175 (3), 1767–1775, URL http://www.ncbi.nlm.nih.gov/entrez/query.fcgi?cmd=Retrieve&db=PubMed&dopt=Citation&list_uids=16034118.
- Diamond, M.S., Sitati, E.M., Friend, L.D., Higgs, S., Shrestha, B., Engle, M., 2003. A critical role for induced IgM in the protection against West Nile virus infection. *J. Exp. Med.* 198 (12), 1853–1862, URL <http://www.ncbi.nlm.nih.gov/articlerender.fcgi?artid=2194144&tool=pmcentrez&rendertype=abstract>.
- Egen, J.G., Rothfuchs, A.G., Feng, C.G., Horwitz, M.A., Sher, A., Germain, R.N., 2011. Intravital imaging reveals limited antigen presentation and T cell effector function in mycobacterial granulomas. *Immunity* 34 (5), 807–819, URL <http://www.ncbi.nlm.nih.gov/pubmed/21596592>.
- Elbert, K.J., Schäfer, U.F., Schäfers, H.J., Kim, K.J., Lee, V.H., Lehr, C.M., 1999. Monolayers of human alveolar epithelial cells in primary culture for pulmonary absorption and transport studies. *Pharm. Res.* 16 (5), 601–608, URL <http://www.ncbi.nlm.nih.gov/pubmed/10349999>.
- Fadel, S., Bromley, S., Medoff, B., Luster, A., 2008. CXCR3-deficiency protects influenza-infected CCR5-deficient mice from mortality. *Eur. J. Immunol.* 38 (12), 3376–3387. <http://dx.doi.org/10.1002/eji.200838628>. CXCR3-deficiency, URL <http://onlinelibrary.wiley.com/doi/10.1002/eji.200838628/full>.
- Gadhamsetty, S., Marée, A.F.M., Beltman, J.B., De Boer, R.J., 2014. A general functional response of cytotoxic T lymphocyte-mediated killing of target cells. *Biophys. J.* 106 (8), 1780–1791.
- Ganusov, V.V., De Boer, R.J., 2008. Estimating in vivo death rates of targets due to CD8 T-cell-mediated killing. *J. Virol.* 82 (23), 11749–11757, URL <http://www.ncbi.nlm.nih.gov/articlerender.fcgi?artid=2583656&tool=pmcentrez&rendertype=abstract>.
- Groom, J.R., Luster, A.D., 2011a. CXCR3 ligands: redundant, collaborative and antagonistic functions. *Immunol. Cell Biol.* 89 (2), 207–215, URL <http://www.ncbi.nlm.nih.gov/pubmed/21221121>.
- Groom, J.R., Luster, A.D., 2011b. CXCR3 in T cell function. *Exp. Cell Res.* 317 (5), 620–631, URL <http://www.ncbi.nlm.nih.gov/articlerender.fcgi?artid=3065205&tool=pmcentrez&rendertype=abstract>.
- Gunn, M.D., Tangemann, K., Tam, C., Cyster, J.G., Rosen, S.D., Williams, L.T., 1998. A chemokine expressed in lymphoid high endothelial venules promotes the adhesion and chemotaxis of naive T lymphocytes. *Proc. Natl. Acad. Sci. U. S. A.* 95 (1), 258–263, URL <http://www.ncbi.nlm.nih.gov/articlerender.fcgi?artid=181938&tool=pmcentrez&rendertype=abstract>.
- Handel, A., Antia, R., 2008. A simple mathematical model helps to explain the immunodominance of CD8 T cells in influenza A virus infections. *J. Virol.* 82 (16), 7768–7772 <http://www.ncbi.nlm.nih.gov/articlerender.fcgi?artid=2519595&tool=pmcentrez&rendertype=abstract>.
- Hojii, A., Rinaldo, C.R., 2005. Human CD8+ T cells specific for influenza A virus M1 display broad expression of maturation-associated phenotypic markers and chemokine receptors. *Immunology* 115 (2), 239–245, URL http://www.ncbi.nlm.nih.gov/entrez/query.fcgi?cmd=Retrieve&db=PubMed&dopt=Citation&list_uids=15885130.
- Hsieh, M.-F., Lai, S.-L., Chen, J.-P., Sung, J.-M., Lin, Y.-L., Wu-Hsieh, B.A., Gerard, C., Luster, A., Liao, F., 2006. Both CXCR3 and CXCL10/IFN-inducible protein 10 are required for resistance to primary infection by dengue virus. *J. Immunol.* 177 (3), 1855–1863, URL <http://www.ncbi.nlm.nih.gov/pubmed/16849497>.
- Ingulli, E., Funatake, C., Jacovetty, E.L., Zanetti, M., 2009. Cutting edge: antigen presentation to CD8 T cells after influenza A virus infection. *J. Immunol.* 182 (1), 29–33, URL <http://www.ncbi.nlm.nih.gov/pubmed/19109130>.
- Julkunen, I., Melén, K., Nyqvist, M., Pirhonen, J., Sareneva, T., Matikainen, S., 2000. Inflammatory responses in influenza A virus infection. *Vaccine* 19 (Supplement 1), S32–7. [http://dx.doi.org/10.1016/S0264-410X\(00\)00275-9](http://dx.doi.org/10.1016/S0264-410X(00)00275-9), ISSN 0264410X, URL http://www.ncbi.nlm.nih.gov/entrez/query.fcgi?cmd=Retrieve&db=PubMed&dopt=Citation&list_uids=11163460.
- Kim, T.S., Sun, J., Braciale, T.J., 2011. T cell responses during influenza infection: getting and keeping control. *Trends Immunol.* 32 (5), 225–231, URL <http://www.ncbi.nlm.nih.gov/pubmed/21435950>.
- Klein, R.S., Lin, E., Zhang, B., Luster, A.D., Tollett, J., Samuel, M.A., Engle, M., Diamond, M.S., 2005. Neuronal CXCL10 directs CD8+ T-cell recruitment and control of West Nile virus encephalitis. *J. Virol.* 79 (17), 11457–11466, URL <http://jvi.asm.org/cgi/content/abstract/79/17/11457>.
- Kohlmeier, J.E., Cookenham, T., Miller, S.C., Roberts, A.D., Christensen, J.P., Thomsen, A.R., Woodland, D.L., 2009. CXCR3 directs antigen-specific effector CD4+ T cell migration to the lung during parainfluenza virus infection. *J. Immunol.* 183 (7), 4378–4384, URL <http://www.ncbi.nlm.nih.gov/articlerender.fcgi?artid=2757292&tool=pmcentrez&rendertype=abstract>.
- Kohlmeier, J.E., Reiley, W.W., Perona-Wright, G., Freeman, M.L., Yager, E.J., Connor, L.M., Brincks, E.L., Cookenham, T., Roberts, A.D., Burkum, C.E., Sell, S., Winslow, G.M., Blackman, M.A., Mohrs, M., Woodland, D.L., 2011. Inflammatory chemokine receptors regulate CD8(+) T cell contraction and memory generation following infection. *J. Exp. Med.* 208 (8), 1621–1634, URL <http://www.ncbi.nlm.nih.gov/pubmed/21788409>.
- Lee, H.Y., Topham, D.J., Park, S.Y., Hollenbaugh, J., Treanor, J., Mosmann, T.R., Jin, X., Ward, B.M., Miao, H., Holden-Wiltse, J., Perelson, A.S., Zand, M., Wu, H., 2009. Simulation and prediction of the adaptive immune response to influenza A virus infection. *J. Virol.* 83 (14), 7151–7165, URL <http://www.ncbi.nlm.nih.gov/articlerender.fcgi?artid=2704765&tool=pmcentrez&rendertype=abstract>.
- Li Jeon, N., Baskaran, H., Dertinger, S.K.W., Whitesides, G.M., Van De Water, L., Toner, M., 2002. Neutrophil chemotaxis in linear and complex gradients of interleukin-8 formed in a microfabricated device. *Nat. Biotechnol.* 20 (8), 826–830, URL <http://www.ncbi.nlm.nih.gov/pubmed/12091913>.
- Lim, K., Hyun, Y.-M., Lambert-Emo, K., Capece, T., Bae, S., Miller, R., Topham, D.J., Kim, M., 2015. Neutrophil trails guide influenza-specific CD+8 T cells in the airways. *Science* 349 (6252), aaa4352.
- Marino, S., Hogue, I.B., Ray, C.J., Kirschner, D.E., 2008. A methodology for performing global uncertainty and sensitivity analysis in systems biology. URL <http://dx.doi.org/10.1016/j.jtbi.2008.04.011>.
- Martin-Fontecha, A., Sebastian, S., Höpken, U.E., Uggioni, M., Lipp, M., Lanzavecchia, A., Sallusto, F., 2003. Regulation of dendritic cell migration to the draining lymph node: impact on T lymphocyte traffic and priming. *J. Exp. Med.* 198 (4), 615–621, ISSN 0022-1007.
- Matsukura, S., Kokubu, F., Noda, H., Tokunaga, H., Adachi, M., 1996. Expression of IL-6, IL-8, and RANTES on human bronchial epithelial cells, NCI-H292, induced by influenza virus A. *J. Allergy Clin. Immunol.* 98 (6 Pt 1), 1080–1087, URL http://www.ncbi.nlm.nih.gov/entrez/query.fcgi?cmd=Retrieve&db=PubMed&dopt=Citation&list_uids=8977509.
- McDonald, B., Pittman, K., Menezes, G.B., Hirota, S.A., Slaba, I., Waterhouse, C.C.M., Beck, P.L., Muruve, D.A., Kubis, P., 2010. Intravascular danger signals guide neutrophils to sites of sterile inflammation. *Science* 330 (6002), 362–366, URL <http://www.sciencemag.org/cgi/doi/10.1126/science.1195491>.
- Medoff, B.D., Thomas, S.Y., Banerji, A., Wain, J.C., Zhang, H., Lilly, C.M., Ginnis, L.C., Luster, A.D., 2005. Pathogenic T-cell recruitment into the airway in human disease. *Ann. N. Y. Acad. Sci.* 1062, 220–241, URL <http://www.ncbi.nlm.nih.gov/pubmed/16461804>.

- Miao, H., Hollenbaugh, J.A., Zand, M.S., Holden-Wiltse, J., Mosmann, T.R., Perelson, A.S., Wu, H., Topham, D.J., 2010. Quantifying the early immune response and adaptive immune response kinetics in mice infected with influenza A virus. *J. Virol.* 84 (13), 6687–6698, URL <http://www.ncbi.nlm.nih.gov/article.fcgi?artid=2903284&tool=pmcentrez&rendertype=abstract>.
- Miller, M.J., Wei, S.H., Cahalan, M.D., Parker, I., 2003. Autonomous T cell trafficking examined in vivo with intravital two-photon microscopy. *Proc. Natl. Acad. Sci. U. S. A.* 100 (5), 2604–2609, URL <http://www.ncbi.nlm.nih.gov/pubmed/14831356>.
- Mirsky, H.P., Miller M.J., Linderman, J.J., Kirschner, D.E., 2011. Systems biology approaches for understanding cellular mechanisms of immunity in lymph nodes during infection. <http://dx.doi.org/10.1016/j.jtbi.2011.06.037>.
- Mitchell, H., Levin, D., Forrest, S., Beauchemin, C.a.a., Tipper, J., Knight, J., Donart, N., Layton, R.C., Pyles, J., Gao, P., Harrod, K.S., Perelson, A.S., Koster, F., 2011. Higher level of replication efficiency of 2009 (H1N1) pandemic influenza virus than those of seasonal and avian strains: kinetics from epithelial cell culture and computational modeling. *J. Virol.* 85 (2), 1125–1135. <http://dx.doi.org/10.1128/JVI.01722-10>, ISSN 1098-5514 URL <http://www.ncbi.nlm.nih.gov/articlerender.fcgi?artid=3019989&tool=pmcentrez&rendertype=abstract>.
- Murillo, L.N., Murillo, M.S., Perelson, A.S., 2013. Towards multiscale modeling of influenza infection. *Journal of theoretical biology* 332, 267–290. <http://dx.doi.org/10.1016/j.jtbi.2013.03.024>.
- Nandagopal, S., Wu, D., Lin, F., 2011. Combinatorial guidance by CCR7 ligands for T lymphocytes migration in Co-existing chemokine fields. *PLoS ONE* 6 (3), 11, URL <http://www.ncbi.nlm.nih.gov/articlerender.fcgi?artid=3064588&tool=pmcentrez&rendertype=abstract>.
- Okada, T., Miller, M.J., Parker, I., Krummel, M.F., Neighbors, M., Hartley, S.B., OG’arra, A., Cahalan, M.D., Cyster, J.G., 2005. Antigen-engaged B cells undergo chemotaxis toward the T zone and form motile conjugates with helper T cells. *PLoS Biol.* 3 (6), e150, URL <http://www.ncbi.nlm.nih.gov/articlerender.fcgi?artid=1088276&tool=pmcentrez&rendertype=abstract>.
- Pawelek, K.A., Huynh, G.T., Quinlivan, M., Cullinane A., Rong, L., Perelson, A.S., 2012. Modeling within-host dynamics of influenza virus infection including immune responses. *PLoS Comput. Biol.* 8 (6).
- Price, I., Mochan-Keef, E.D., Swigon, D., Ermentrout, G.B., Lukens, S., Toapanta, F.R., Ross, T.M., Clermont, G., 2015. The inflammatory response to influenza A virus (H1N1): an experimental and mathematical study. *J. Theor. Biol.* 374, 83–93. <http://dx.doi.org/10.1016/j.jtbi.2015.03.017>, ISSN 1095-8541, URL <http://www.sciencedirect.com/science/article/pii/S0022519315001265>.
- Saenz, R.A., Quinlivan, M., Elton, D., MacRae, S., Blunden, A.S., Mumford, J.A., Daly, J. M., Digard, P., Cullinane, A., Grenfell, B.T., McCauley, J.W., Wood, J.L.N., Gog, J.R., 2010. Dynamics of influenza virus infection and pathology. *J. Virol.* 84 (8), 3974–3983, URL <http://www.ncbi.nlm.nih.gov/pubmed/20130053>.
- Textor, J., Henrickson, S.E., Mandl, J.N., von Andrian, U.H., Westermann, J., de Boer, R.J., Beltman, J.B., 2014. Random migration and signal integration promote rapid and robust T cell recruitment. *PLoS Comput. Biol.* 10 (8), e1003752, ISSN 1553-7358, URL <http://www.ncbi.nlm.nih.gov/pubmed/25102014>.
- Thapa, M., Welner, R.S., Pelayo, R., Carr, D.J.J., 2008. CXCL9 and CXCL10 expression are critical for control of genital herpes simplex virus type 2 infection through mobilization of HSV-specific CTL and NK cells to the nervous system. *J. Immunol.* 180 (2), 1098–1106, URL <http://www.ncbi.nlm.nih.gov/articlerender.fcgi?artid=2185792&tool=pmcentrez&rendertype=abstract>.
- Vroomans, R.M.A., Marée, A.F.M., De Boer, R.J., Beltman, J.B., 2012. Chemotactic migration of T cells towards dendritic cells promotes the detection of rare antigens. *PLoS Comput. Biol.* 8 (11), e1002763. <http://dx.doi.org/10.1371/journal.pcbi.1002763>.
- Wareing, M.D., Lyon, A.B., Lu, B., Gerard, C., Sarawar, S.R., 2004. Chemokine expression during the development and resolution of a pulmonary leukocyte response to influenza A virus infection in mice. *J. Leukoc. Biol.* 76 (4), 886–895, URL <http://www.ncbi.nlm.nih.gov/pubmed/15240757>.
- Warrender, C., Forrest, S., Koster, F., 2006. Modeling intercellular interactions in early Mycobacterium infection. *Bull. Math. Biol.* 68 (8), 2233–2261, URL <http://www.ncbi.nlm.nih.gov/pubmed/17086496>.
- WHO Influenza Fact Sheet. Technical Report, World Health Organisation, 2009.
- Wu, C.F.J., Jackknife, 1986. Bootstrap and other resampling methods in regression analysis. *Ann. Stat.* 14 (4), 1261–1295. <http://dx.doi.org/10.1214/aos/1176350142>, ISSN 00905364, URL <http://projecteuclid.org/euclid-aos/1176350142>.
- Wuest, T.R., Carr, D.J.J., 2008. Dysregulation of CXCR3 signaling due to CXCL10 deficiency impairs the antiviral response to herpes simplex virus 1 infection. *J. Immunol.* 181 (11), 7985–7993, URL <http://www.ncbi.nlm.nih.gov/articlerender.fcgi?artid=2596651&tool=pmcentrez&rendertype=abstract>.
- Zeng, H., Pappas, C., Katz, J.M., Tumprey, T.M., 2011. The 2009 pandemic H1N1 and triple-reassortant swine H1N1 influenza viruses replicate efficiently but elicit an attenuated inflammatory response in polarized human bronchial epithelial cells. *J. Virol.* 85 (2), 686–696, URL <http://www.ncbi.nlm.nih.gov/pubmed/21047961>.
- Zhao, M.Q., Stoler, M.H., Liu, A.N., Wei, B., Soguero, C., Hahn, Y.S., Enelow, R.I., 2000. Alveolar epithelial cell chemokine expression triggered by antigen-specific cytolytic CD8(+) T cell recognition. *J. Clin. Investig.* 106 (6), R49–R58, URL <http://www.ncbi.nlm.nih.gov/articlerender.fcgi?artid=381394&tool=pmcentrez&rendertype=abstract>.
- Zheng, H., Jin, B., Henrickson, S.E., Perelson, A.S., Von Andrian, U.H., Chakraborty, A.K., 2008. How antigen quantity and quality determine T-cell decisions in lymphoid tissue. *Mol. Cell. Biol.* 28 (12), 4040–4051, URL <http://www.ncbi.nlm.nih.gov/articlerender.fcgi?artid=2423119&tool=pmcentrez&rendertype=abstract>.

A spatial model of the efficiency of T cell search in the influenza-infected lung (SUPPLEMENT)

Drew Levin^{1,*}, Stephanie Forrest¹, Soumya Banerjee¹, Candice Clay², Judy Cannon³, Melanie Moses¹, Frederick Koster^{1,2}

1 Department of Computer Science, University of New Mexico, Albuquerque, NM, USA

2 Lovelace Respiratory Research Institute, Albuquerque, NM, USA

3 Department of Molecular Genetics & Microbiology Department of Pathology, University of New Mexico Health Sciences Center, Albuquerque, NM, USA

* E-mail: Corresponding drew@cs.unm.edu

1 Models

1.1 CyCells implementation details

The CyCells modeling environment splits its populations into two types: cells and molecules. Cells are considered to be unique agents and are modeled individually. Conversely, molecules are represented as compartmentalized concentrations. These compartments are arranged as a grid that covers the environment. Each square in the grid contains a unique concentration of the given molecule. Each type of molecule is represented in a unique grid.

Molecular behavior is limited to diffusion and decay. At each time step, CyCells decreases the concentration of each square in the grid according to the decay rate specified for the given molecule. CyCells then diffuses the molecules by applying a discrete diffusion equation to each grid square, taking into account the specified diffusion constant and the concentrations in neighboring squares.

New molecules can be secreted by cell objects, such as an infected cell secreting new virus. In this scenario CyCells calculates the amount of virus secreted per time step, based upon the cell's defined production rate, and then adds this quantity to the grid square that overlaps the secreting cell. If a cell ingests a molecule, it will subtract the appropriate concentration from the grid square it overlaps. If the concentration at that square is not enough to represent a full molecule, concentration will be removed from neighboring squares in an ever expanding diamond until the total concentration is equal to a single molecule.

Cells will measure the local concentration at their position by calculating a linearly interpolated

combination of the concentrations in the grid squares surrounding the cell in instances where cell behavior depends on the local molecular concentration.

1.2 Model implementation details

An overview of the model implementation is shown in Fig. 2. The model is initialized with one virus-secreting cell placed in the middle of a 2-dimensional sheet of hexagonally-tiled epithelial cells (288,212 total cells). The sheet measures 5mm per side, which is large enough to contain the infection (Fig. 5). The molecular grid (Text S1 1.3) is initialized with a resolution of 20 μm . Each time step of the model represents 6 seconds.

Healthy cells transition to virus-incubating based on a probability that scales linearly with the local virus concentration. When a cell ‘becomes infected’ it removes the amount of viral concentration equal to a single virion.

Virus-incubating cells idle for 10 hours (with standard deviation $\sigma = 1$ hour) and then transition to virus-secreting cells. Virus-incubating cells also begin to secrete chemokine after 8 hours (except for aH5N1 which only secretes RANTES after a 16 hour delay).

Virus-secreting cells secrete both virus and chemokine (the RANTES portion of the chemokine production is added in 16 hours after the initial infection) and die after 1,000 minutes of production (16.7 hours). Virus-secreting cells will also probabilistically transition to apoptizing cells in the presence of T cells (defined by the existence of a T cell within 2 μm). The number of T cells in the vicinity of the virus-secreting cell has no effect on the rate that apoptosis is induced in the model.

Apoptizing cells secrete virus and chemokine for one hour and then die.

T cells are added to the model at a constant rate of 1,257 per hour (Text S1 2.1). Because the model environment is only a small portion of the entire lung (0.25%), most of the T cells miss the model window and are not visually represented. The T cells that miss recirculate and enter the lung at a new random location after a delay of six seconds.

The cells that enter the model window are placed at a random position and immediately check the local chemokine concentration. If the concentration is above the sensitivity threshold, the T cells immediately transition to the chemotaxing state. If not, the T cells recirculate and reenter the lung in a new location after a six second delay. Recirculating T cells have a probabilistic decay rate that corresponds to a 3 day lifespan. Recirculating T cells are not visually represented.

Chemotaxing T cells move directly up the chemokine gradient until they find a local concentration maximum. T cells probabilistically decay at a rate corresponding to a 2 hour lifespan. Chemotaxing T cells have no effect other than inducing apoptosis in virus-secreting cells by proximity.

1.3 Modeling decisions

1.3.1 Two dimensional lung

We model the lung as a two-dimensional system for several reasons. Unlike the lymph node where dendritic cells and T cells navigate a three-dimensional volume, lung infection dynamics are confined to a thin tissue between capillary endothelial cells and alveolar epithelial cells. Although these alveoli are segregated by the lung's acinar structure on a small scale, we do not represent this in the model because the spreading of influenza eventually ignores the boundaries between acinii. Therefore our model does not incorporate this small-scale level of segregation.

1.3.2 Uniform blood flow

Our model assumes that blood flows uniformly through the lung vascular network. It is possible that blood flow is increased in the direction of an infected region of the lung by local inflammation. Thus our model may underestimate the recruitment efficiency of local inflammation and hyperemia. If this is indeed the case, our model underestimates the effect of the immune response.

2 Results

2.1 T cell sensitivity to chemokine

The model simulates a chemokine gradient surrounding the infected focus (Fig. 5), based on the calculated per-infected cell secretion rate (Table 1) and known chemical parameters for a 10 kDa protein (Table 2). T cell sensitivity depends on receptor density (Desmetz et al., 2006) and this was assumed to be constant.

Because this parameter is unknown, we simulated T cell sensitivity levels ranging over 10 orders of magnitude. Concentration-dependent behavior of cells responding to chemokine was the same over a wide range of concentrations from 0.01 pg/mL to 100 ng/mL (model variance is discussed in the main text). Decreased recruitment was predicted only by supra-natural concentration sensitivity levels at and above

$1 \mu\text{g/mL}$. We then set the sensitivity to 100 ng/mL for all future runs (10 nM concentration assuming a chemokine molecular weight of 10 kDa) (Gao et al., 2003).

2.2 Chemokine combinations

Because aH5N1 has been shown to suppress the production of interferon (Mitchell et al., 2011), we consider that IP-10 production is markedly reduced in comparison with that of RANTES and this may lead to elevated RANTES secretion measured in aH5N1 *in vitro* infection when compared to the other strains. Thus, IP-10 production was not included in aH5N1 simulations.

T cell sensitivity depends on receptor density (Desmetz et al., 2006) and this was assumed to be constant. Thus, the chemokines in combination work additively in our model.

Four models runs (both, IP-10, RANTES, and none) were performed for sH1N1 and pH1N1 strains and two runs (RANTES and none) for aH5N1. The runs show how the presence and/or absence of specific chemokines affect the simulated immune response (Fig. S3). The lack of both chemokines leads to runaway infections in all three strains. The presence of only RANTES is enough to contain the aH5N1 infection, but is weaker than IP-10 in both H1N1 strains. In sH1N1 and pH1N1 simulations, IP-10 alone proves to be as effective as the combination of IP-10 and RANTES. This suggests that RANTES does not play a significant role in infections that stimulate an IP-10 response due to the higher production rates of IP-10.

2.3 One-factor-at-a-time sensitivity analysis

A general sensitivity analysis serves two purposes. First, it allows us to observe how the model behavior changes as a single parameter is varied. Second, it allows us to examine which parameters affect the model strongly and which do not. Here we describe the sensitivity analysis of 16 of our parameters in detail.

The model parameters were chosen from literature when available and estimated within plausible ranges otherwise (Tables 1 and 2). One-factor-at-a-time (OFAT) analysis was performed by varying Individual parameters over ranges of plausible (and sometimes even implausible) values while the rest of the parameter set was held constant. Each parameter was varied over all three influenza strains, creating three sets of sensitivity plots (Figures S4-S6).

We then categorized the model parameters into one of three qualitative groups: parameters that do not affect the model's qualitative behavior (stable parameters), parameters that affect the model's quantitative peak infection size but do not affect final clearance, (peak change parameters), and those parameters that affect the final clearance of the infection (sensitive parameters) (Table 3). Parameters are presented along with their range using the following format:

Parameter Name: [*min* — *default* — *max*].

2.3.1 Stable Parameters

Stable parameters do not affect the outcome of the infection unless they are adjusted to values outside the realm of possibility. Specifically, the plausible parameter values in this group are within a range that does not significantly affect the asymptotic behavior of the model. We further split this group into two categories in Table 3, *stable* parameters and *bounded stable* parameters. *Bounded stable* parameters are only stable within a specific range of values, while *stable* parameters seem to be stable over all the values that were tested.

Of interest, this group can be split into two types of parameters: those governing chemokine behavior (chemokine decay, chemokine diffusion, and chemokine secretion) and those governing T cell behavior (T cell circulation time, T cell kill rate, T cell velocity, and the two T cell decay rates). Only the apoptosis time parameter does not fit into one of these two groups, and its inclusion as a stable parameter may be suspect due to the limited range of the values tested. The importance of the apoptosis time parameter is discussed in more detail in the main results section: Temporal Effects.

The stability of these parameters makes sense in the context of our model. Chemokine exists in our model to provide a chemical gradient that T cells may follow to the focus of infection. The total quantity of the chemokine in the lung does not have a strong effect on the location and size of the gradient. Thus, the model will be stable for any values of chemokine secretion, diffusion, and decay that provide a gradient that T cells are able to follow.

Similarly, T cells affect the model by clearing cells expressing virus. As discussed in the main paper, the chemokine gradient creates areas of maximal concentration that attract all the T cells inside its basin of attraction. Thus, most T cells are attracted to the same areas of the infection and overlap considerably. Increasing T cell numbers and efficiency will not help clear the infection beyond a certain point.

While we have claimed that these parameters are qualitatively stable within a certain range, many of the parameters were set to values that did lead to a divergent model behavior. Testing these extreme values provides bracketing information regarding the range of stability of the parameter in question. We have deemed these deviations acceptable on an individual basis as described below.

Compartmental modeling design suggests the removal of such stable parameters. Due to the nature of the ABM, inclusion of these parameters is mechanistically necessary. Thus, we include and parameterize them using the methods described in the main paper and Table 2.

Apoptosis Time: [$0 — 1h — 2h$] - Apoptosis time describes how long it takes for a cell to complete apoptosis and transition to an inert dead state.

We chose to limit the increase of the apoptosis to a factor of two because larger values would not be biologically relevant. We considered values as low as zero.

Adjusting the apoptosis time causes the model results to diverge slightly in the sH1N1 strain (Fig. S5). Also of interest, reducing the apoptosis time to zero still did not allow the immune response to clear the pandemic infection. As stated earlier, its inclusion in this group is marginal and its effects are described in more detail in the results section of the main paper.

Chemokine Decay Rate: [$3e-6 Hz — 3e-4 Hz — 3e-2 Hz$] - The chemokine decay rate defines how quickly the chemokine is removed from the system. A higher rate of decay corresponds to a quicker rate of removal.

We tested values up to two orders of magnitude larger and smaller than the default parameter value even though these extremes are not biologically plausible.

Varying the chemokine decay rate results in stable model behavior for values one order of magnitude larger and smaller than the default. A value two orders of magnitude smaller results in divergent behavior for both the aH5N1 strain and the sH1N1 strain and a value two orders of magnitude larger results in divergent behavior for only the sH1N1 strain. This maximum decay rate used for all three strains corresponds to an implausible 18 second half-life. The minimal value corresponds to a similarly implausible 50 hour half-life. The fact that an extremely low decay rate can hinder clearance is interesting. In this case, lack of decay allows the chemokine to diffuse homogeneously across the entire infection, removing the concentration gradient required by T cells to find the active areas of the infection. This suggests that

the quantity of chemokine is immaterial so long as there is enough for T cells to be able to detect it.

Chemokine Diffusion Rate: [$3e-3 \mu\text{m}^2/\text{s}$ — $0.3 \mu\text{m}^2/\text{s}$ — $30 \mu\text{m}^2/\text{s}$] - The chemokine diffusion rate regulates how quickly the chemokine molecules spread out over the infected region. A larger diffusion coefficient corresponds to a more rapid rate of spread.

We tested values up to two orders of magnitude larger and smaller than the default parameter value.

The chemokine diffusion rate only diverges in the aH5N1 strain for the highest value. Our estimate for the diffusion rate is already elevated as it is optimistically based off of the Stokes-Einstein equation using viscosity of water.

Chemokine Secretion Rate: [$1e-7 \text{ pg}/\text{s}\cdot\text{cell}$ — $1e-5 \text{ pg}/\text{s}\cdot\text{cell}$ — $1e-3 \text{ pg}/\text{s}\cdot\text{cell}$] - The chemokine secretion rate defines how much chemokine each infected cell secretes per second.

We tested values up to two orders of magnitude larger and smaller than the default parameter value.

Chemokine secretion values differ between strains. It is important to note that aH5N1 and sH1N1 show a threshold at the same concentration: near $1e-6 \text{ pg}/\text{s}\cdot\text{cell}$. This is an artifact of our artificially selected chemokine detection threshold, detailed in section S2.1 and Figure S2. Because we initially picked a sensitivity threshold near the edge of the stable range of possible values, decreasing the total concentration of chemokine inadvertently crosses that arbitrary threshold and does not necessarily suggest an actual region of divergence.

T Cell Circulation Time: [1s — 6s — 1h] - T cell circulation time defines how long a T cell takes to recirculate through the vascular system when it does not encounter the infection as it passes through the lung. This value should correspond to the vascular circulation time of a mouse as we used a mouse-sized model for computational reasons.

A value of 1 second was chosen as the minimum due to computational constraints, yet this value is likely already too small to be biologically plausible. We extended the range to up to 600 times the default value to examine what happens when the circulation time is so long that the T cells are effectively removed from the simulation if they miss the focus of infection on their first pass through the lung.

T cell circulation times were tested over a very large range and does diverge for high values. Classifying this parameter as *bounded stable* may seem counterintuitive when examining the sensitivity figures. It is important to note that in this case, we tested extra values on the higher end of the baseline than

other plots. While each strain does show divergence beyond a certain value, the intermediate values of 1 second and 20 seconds remain qualitatively similar to the main result, demonstrating a stable range surrounding the default value. Because vascular and lymph circulation times are unknown, parameter values of up to 1 minute and 3 minutes in mice may be plausible and warrant further study.

T Cell Expected Kill Time: [$0m — 10m — 100m$] - The T cell expected kill time defines the rate at which T cells probabilistically induce apoptosis of virus-expressing epithelial cells in their immediate vicinity. A lower kill time corresponds to a higher kill rate.

We tested values only one order of magnitude higher than the default limiting the time to induce apoptosis of a virus-expressing cell to one hour. On the other side, we allowed T cells to induce apoptosis instantly to see if any delay in the induction of apoptosis was responsible for the inability for the immune response to clear the pandemic infection.

The parameter only diverges on the higher end in sH1N1. The extreme value corresponds to a T cell needing 100 minutes to induce the apoptosis of a single infected cell and is not biologically reasonable. The intermediate value corresponds to a time of 33.3 minutes and is also unlikely. Of interest, removing the parameter entirely by setting the kill time to instant was still not enough to allow the immune response to clear the pandemic infection.

T Cell Speed: [$3.6 \mu\text{m}/\text{h} — 6 \mu\text{m}/\text{m} — 10 \mu\text{m}/\text{s}$] - T cell speed determines how fast T cells move over the epithelial monolayer.

We tested values up to two orders of magnitude larger and smaller than the default parameter value. Divergence does occur in sH1N1 for the extreme values on both ends (but not for the intermediate ones). T cell movement in tissue has been observed (Egen et al., 2011). Thus, we consider the extreme values biologically implausible.

T Cell Age in Blood: [$1h — 4d — 400d$] - The expected age determines the decay rate of T cells in blood.

We tested values up to two orders of magnitude larger and smaller than the default parameter value. T cell decay parameters allow the model to diverge only in the most extreme cases. Neither of these values are reasonable and the parameters show stable behavior otherwise. The default parameter appears

to define a model as effective at clearing the infection as models with much larger values.

T Cell Age at FOI: [$12m - 2h - 20h$] - The expected age determines the decay rate of T cells at the focus of infection (FOI).

We tested values up to one order of magnitude larger and smaller than the default parameter value.

T cell decay parameters allow the model to diverge only in the most extreme cases. Neither of these values are reasonable and the parameters show stable behavior otherwise. While the default of 2 hours may seem short, it appears to generate similar behavior to models with larger values.

T Cell Production Rate: [$125 \text{ cells}/h - 1257 \text{ cells}/h - 3750 \text{ cells}/h$] - The T cell production rate determines the rate at which T cells enter the blood stream starting at day 5 post-infection.

We tested values up to three times larger and ten times smaller than the default value. Values beyond a three-fold increase were not computationally tractable.

The T cell production rate does have a consistent response over its different values, but this effect is minimized above a certain rate. Thus, it is reasonable to assume that there is a threshold of T cell production beyond which the dynamics of the infection do not change. This is consistent with our observations of T cell clumping in areas of high chemokine concentration. Increasing the number of T cells in the system does not control the infection beyond a certain point because the T cells overlap in space and become redundant. The rapid decline of the infection size for the maximum value of $3\mu\text{m}^2/\text{s}$ is simply an artifact of the infection exhausting the entire model space by day 3.

2.3.2 Difference in Peak Only

Difference in peak only parameters affect the model's behavior up until the introduction of the T cell response, followed by a return to similar day 10 outcomes. Interestingly, these are the two parameters that define the transition delay between the different stages of epithelial cell infection. Because these terms refer to the timing of when infected cells release the virus particles, neither one directly affects the kinetics of the virus itself and thus the infection's behavior is still determined by the properties of the virus and the T cell response.

Incubation Delay: [$5h - 10h - 20h$] - Incubation delay describes how long an epithelial cell

takes to transition to the virus-expressing state after it is initially infected. During this period, the cell, while infected, does not secrete virus.

We tested values up to a factor of two larger and smaller than the original parameter setting.

While a longer incubation time does not change the number of virions released by each infected cell, it does slow down the spread of the infection. Conversely, a shorter incubation time allows the infection to spread more quickly by allowing the infected cell to release the new virus in to the system earlier. Thus, changes in the incubation time do affect the infection profile before the introduction of T cells. The infection dynamics change dramatically upon the arrival of T cells. One of the main factors in determining whether or not the infection is cleared is the amount of new virus produced per infected cell. While this does depend somewhat on the overall size of the plaque, this value depends heavily on shutting down the expression of new virus, something T cells are unable to do during the cellular incubation phase as the virus-incubating cell has not expressed virus for T cells to detect. Thus, assuming the original plaque has not grown so large that it can no longer be effectively covered by the T cell response, the overall course of the infection will be unaffected by the length of the incubation period.

Expression Delay: [$100m — 1,000m — 50h$] - The expression delay is the amount of time a virus secreting cell will secrete virus in the absence of a T cell intervention. At the end of this time period, the expressing cell will transition to the dead state and remain inert for the remainder of the simulation.

The parameter was increased up by a factor of 3 and down by a factor of 10. In each case, the change is extreme enough that the resulting values are not biologically likely.

Adjusting this parameter seems to affect the model behavior up until the arrival of the T cell response, after which the model converges back to the baseline behavior. This effect occurs because once T cells arrive, virus secreting cells no longer survive for their full lifespan. Rather, the delay becomes limited by the apoptosis time parameter.

2.3.3 Sensitive Parameters

Sensitive parameters directly affect the result of the infection. There are five parameters classified as sensitive: viral response to IgM, infectivity, T cell production rate, viral decay, and viral diffusion. By comparing the three strains of influenza, we also know that the viral secretion rate affects the result. Of interest, a majority of these parameters are related to the behavior of the virus. The only sensitive

parameter not related to the behavior or the virus is the T cell production rate.

Viral Response to IgM: [$1 — 10 — 1,000$] - Viral response to IgM simulates the presence of IgM at day 4 post-infection by increasing the decay rate of free virus particles by the given factor.

We examined a very large range of values, from the lowest possible value of 1 (effectively removing IgM), to an increased decay rate of three orders of magnitude.

While it is true that the extreme values have a large effect on the model behavior, it is more of interest that the intermediate values also seem to change the model behavior. This shows that there is no stable area around the default as is seen in the *bounded stable* parameters. The higher the strength of this parameter, the less virus there is in the system. Because the true effective strength of IgM is unknown in the context of this model, it is not a target of our investigation.

Viral Decay Rate: [$1e-7 \text{ Hz} — 1e-5 \text{ Hz} — 1e-3 \text{ Hz}$] - Viral decay determines how quickly free virus is removed from the system. A larger decay rate corresponds to faster removal.

We tested values up to two orders of magnitude larger and smaller than the default parameter value.

Viral decay has the exact same effect as the viral response to IgM parameter. Its value directly determines how much virus remains in the system over the course of the infection. There is a strong relationship between the decay rate and the resulting infection profile across all values tested.

Infectivity: [$12 \text{ m/virion} — 2 \text{ h/virion} — 20 \text{ h/virion}$] - Infectivity describes the ability of the virus to infect healthy cells. A larger value corresponds to a virus particle needing less time to infect a nearby healthy epithelial cell.

We tested values up to one order of magnitude larger and smaller than the default parameter value.

The strength of the infectivity parameter is directly related to how much virus is present in the area of the healthy cells. Thus, viral density is linearly proportional to infectivity. Thus, it behaves similarly to the IgM and viral decay parameters as it directly determines the virulence of the virus.

Viral Secretion Rate: [$5.4e-5 \text{ PFU/s} \cdot \text{cel} — 3.8e-4 \text{ PFU/s} \cdot \text{cel} — 5.1e-3 \text{ PFU/s} \cdot \text{cel}$] - The viral secretion rate determines how quickly virus-secreting epithelial cells secrete new virus particles.

An explicit sensitivity analysis was not directly performed. The range of the parameters are taken

from the respective secretion rates of the aH5N1, sH1N1, and pH1N1 influenzas (Table 1).

The viral secretion rate has a strong effect on the outcome of the infection. Similar to the previously discussed parameters, its value directly affects how much virus there is in the system. Thus, its effect is similar to the previous parameters.

Viral Diffusion Rate: [$3e-4 \mu\text{m}^2/\text{s}$ — $3e-2 \mu\text{m}^2/\text{s}$ — $3 \mu\text{m}^2/\text{s}$] - The viral diffusion rate controls how quickly the virus spreads across the monolayer.

We tested values up to two orders of magnitude larger and smaller than the default parameter value.

The viral diffusion rate does not change how much virus there is in the system. Rather, it determines how fast the virus may spread across the alveoli. While its mechanism is different, its effect may be even stronger than the previous parameters. Increasing the viral diffusion rate so that the virus diffuses faster than the chemokine (an unlikely scenario) allows the virus to out-pace the body's ability to establish a chemical gradient around the infected cells. In this scenario T cells are constantly directed to locations behind the rapidly spreading viral cloud and would be unable to 'get ahead' of the infection.

2.4 Partial rank correlation coefficient sensitivity analysis

We performed a partial rank correlation coefficient (PRCC) sensitivity analysis to complement our one factor at a time (OFAT) parameter analysis. Due to computational limitations, we computed PRCC values only for the sH1N1 strain, confirming that the results of the PRCC are consistent with the conclusions of the original sensitivity analysis and that viral parameters dominate the model output.

2.4.1 PRCC Design and Implementation

PRCC analysis was performed as described in Marino et al. (2008). Samples were generated using Latin hypercube sampling (LHS) to generate 333 sample points for 17 parameters (those from Table 3, plus the sH1N1 viral secretion rate). Each parameter was assigned a confidence distribution (Table S5) and sampled using its inverse cumulative distribution function to generate points with density proportional to the underlying probability distribution function. Each sample point was evaluated three times using unique random seeds for a total of 999 samples. One sample point resulted in undefined model behavior and was removed, leaving a total of 996 samples.

Output is defined as the number of infected cells remaining for each time point. Each model run generates 144,001 time points (10 day model with 6 second time steps). PRCC analysis was performed over every 100th time point, resulting in a time series of 1441 Spearman rank correlation coefficients (ρ) and significance values (p) for each parameter (Figs. S7 - S8).

2.4.2 PRCC Results

The analysis confirmed the conclusion of original sensitivity analysis that viral parameters dominate model output. Of the 17 parameters tested with PRCC analysis, 7 show significance of $p < 0.01$ over the time period where the parameter was relevant to model dynamics (Figs. S6 - S7). All five of the viral parameters (viral response to IgM, viral infectivity, viral decay rate, viral diffusion rate, and viral secretion rate) are significant. Infected cell expression time and the T cell age at the focus of infection are also significant at $p < 0.01$ (but have ρ values near 0). Viral infectivity, viral decay rate, viral diffusion rate, and viral secretion rate are the only parameters that have maximum absolute values of ρ above 0.5. Other parameters showed significant correlations (with low values of ρ), but only over time periods where they were not active.

Viral infectivity, viral diffusion rate, and viral secretion rate, values of ρ cross or approach zero over time. This merely reflects that the modeled target cells have died (Fig. S9) and so the decline in ρ is irrelevant.

2.5 Window of Control

We predict viral control in the model by approximating R_0 and determining if the value is above or below a value of one. R_0 is calculated as the number of virions produced by each cell multiplied by the number of cells infected by each virion. The first half of this equation is the rate of viral production multiplied by the time the cell produces virus. The second part of the equation is termed the viral efficiency rate, E . The equation here is repeated from the main paper:

$$R_0 = p \times (T_{arr} + T_{kill} + T_{apop}) \times E \quad (1)$$

In the main paper, $E(t)$ is approximated as 0.27, and this value is accurate enough to provide useful predictions. Calculating the true value for $E(t)$ is more difficult as it depends on many factors, including

the area of the plaque, the depth of the ring of infected (but not dead cells) around the plaque, the local viral density, and the arrival rate and effectiveness of T cells. Each of these factors change during the infection.

To find values of $E(t)$ for each of the three strains we reran the model in the absence of T cells and calculated the amount of virus that infects cells, $I(t)$, and the amount that decays $D(t)$, at each time step. The viral effectiveness rate is then calculated to be

$$E(t) = \frac{I(t)}{I(t) + D(t)} \quad (2)$$

This approach accounts for the factors listed above and provides a unique measure of $E(t)$ at each point in time. We focus on results in the model after day 5 p.i. corresponding to the arrival of T cells in the main model. In each simulation $I(t)$ remains relatively constant, while $D(t)$ increases linearly with time. We perform least-squared regressions on $I(t)$ and $D(t)$ for each strain and combine the results to give an estimate for $E(t)$ (Table S6).

We use the estimated values of $E(t)$ to calculate R_0 values for each strain in the absence of T cell mediated apoptosis. Because all three $E(t)$ values all change by less than 10% over the five day window, we estimate R_0 values using the average $E(t)$ value for each strain (Table S6). The three strains show similar values for R_0 , suggesting a saturation of viral effectiveness as the plaque grows. This is not the case early in the infection as pH1N1 growth clearly outpaces sh1N1 which in turn expands more rapidly than aH5N1. In the main model, the T cell response limits viral production time, which in turn increases the effectiveness of the virus that is produced. Thus, it is reasonable to assume viral effectiveness remains high in the presence of the T cell response. By accounting for basic spatial and temporal effects as described in the main paper, we approximate $E(t)$ as 0.27 over the course of the infection.

Videos

Videos can be found at the following web address: <http://cs.unm.edu/\%7Edrew/chemokine>

References

- C. Desmetz, Y.-L. Lin, C. Mettling, P. Portalès, H. Rabesandratana, J. Clot, P. Corbeau, The strength of the chemotactic response to a CCR5 binding chemokine is determined by the level of cell surface CCR5 density., *Immunology* 119 (4) (2006) 551–61, ISSN 0019-2805, doi:10.1111/j.1365-2567.2006.02470.x, URL <http://www.ncbi.nlm.nih.gov/articlerender.fcgi?artid=2265826&tool=pmcentrez&rendertype=abstract>
- P. Gao, X.-y. Zhou, Y. Yashiro-ohtani, Y.-f. Yang, N. Sugimoto, S. Ono, T. Nagasawa, H. Fujiwara, T. Hamaoka, The unique target specificity of a nonpeptide chemokine receptor antagonist : selective blockade of two Th1 chemokine receptors CCR5 and CXCR3 cated in their migration to sites of inflammation ., *Journal of Leukocyte Biology* 73 (February) (2003) 273–280, doi:10.1189/jlb.0602269.Journal.
- H. Mitchell, D. Levin, S. Forrest, C. a. a. Beauchemin, J. Tipper, J. Knight, N. Donart, R. C. Layton, J. Pyles, P. Gao, K. S. Harrod, A. S. Perelson, F. Koster, Higher level of replication efficiency of 2009 (H1N1) pandemic influenza virus than those of seasonal and avian strains: kinetics from epithelial cell culture and computational modeling., *Journal of virology* 85 (2) (2011) 1125–35, ISSN 1098-5514, doi:10.1128/JVI.01722-10, URL <http://www.ncbi.nlm.nih.gov/articlerender.fcgi?artid=3019989&tool=pmcentrez&rendertype=abstract>
- J. G. Egen, A. G. Rothfuchs, C. G. Feng, M. A. Horwitz, A. Sher, R. N. Germain, Intravital imaging reveals limited antigen presentation and T cell effector function in mycobacterial granulomas., *Immunity* 34 (5) (2011) 807–819, URL <http://www.ncbi.nlm.nih.gov/pubmed/21596592>.
- S. Marino, I. B. Hogue, C. J. Ray, D. E. Kirschner, A methodology for performing global uncertainty and sensitivity analysis in systems biology, doi:10.1016/j.jtbi.2008.04.011, 2008.
- H. Miao, J. A. Hollenbaugh, M. S. Zand, J. Holden-Wiltse, T. R. Mosmann, A. S. Perelson, H. Wu, D. J. Topham, Quantifying the early immune response and adaptive immune response kinetics in mice infected with influenza A virus., *Journal of Virology* 84 (13) (2010) 6687–6698, URL <http://www.ncbi.nlm.nih.gov/articlerender.fcgi?artid=2903284&tool=pmcentrez&rendertype=abstract>
- R. H. Peters, The ecological implications of body size, vol. Cambridge, Cambridge University Press, ISBN 052128886X, URL <http://books.google.com/books?id=OYVxiZgTXWsC>, 1983.

Figure Legends

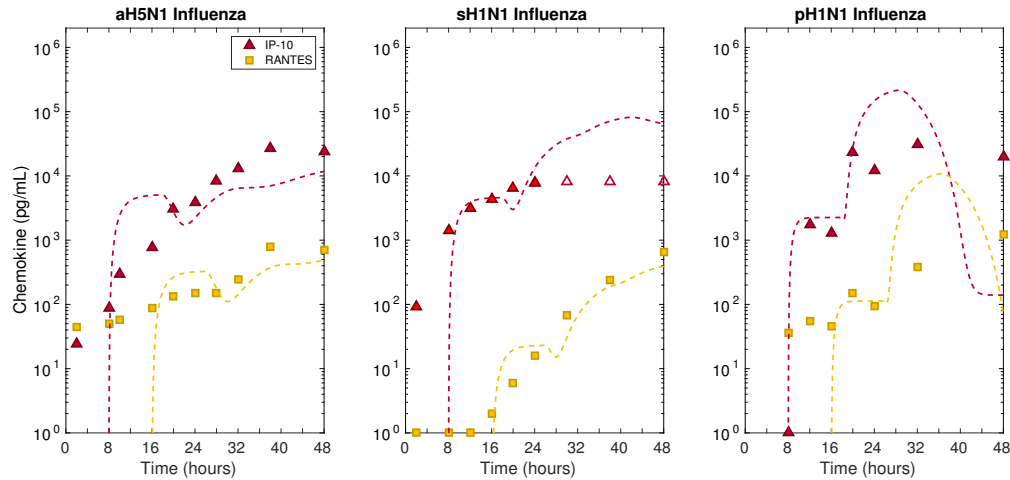


Figure S1. Preliminary Model 1 fits to data. Preliminary Model 1 (Eq. 1) was fit to experimental data (Table S1) using a genetic algorithm as described in the main paper. sH1N1 IP-10 secretion exceeded measurement accuracy above 8500 pg/mL and these three values (empty red triangles) were not included in the model fitting. RMSE values of the fits can be seen in Table S3. IP-10 data and model fits shown in red (triangles), RANTES data and model fits shown in yellow (squares).

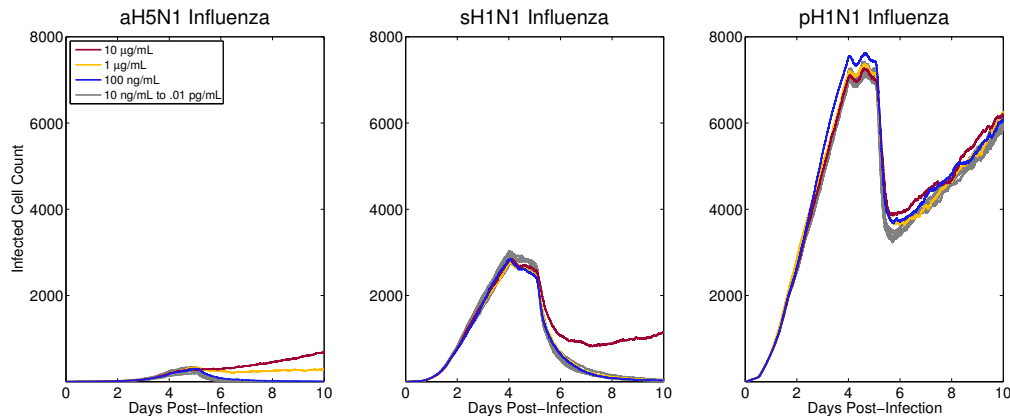


Figure S2. Varying T cell sensitivity to chemokine. H5N1 model results use RANTES only, and sH1N1 and pH1N1 use both IP-10 and RANTES. Total number of incubating, secreting and apoptotic cells are plotted for each infection. The sensitivity value specifies the minimum level of chemokine concentration required for T cells to detect it.

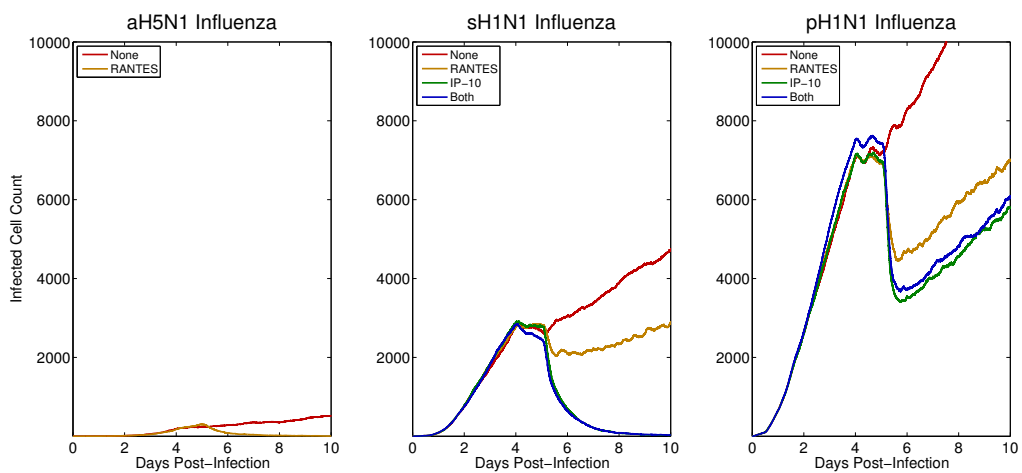


Figure S3. Effects of different chemokine combinations. A) aH5N1 does not stimulate an IP-10 response. B-C) sH1N1 and pH1N1 show no significant difference between IP-10 alone versus IP-10 and RANTES combined.

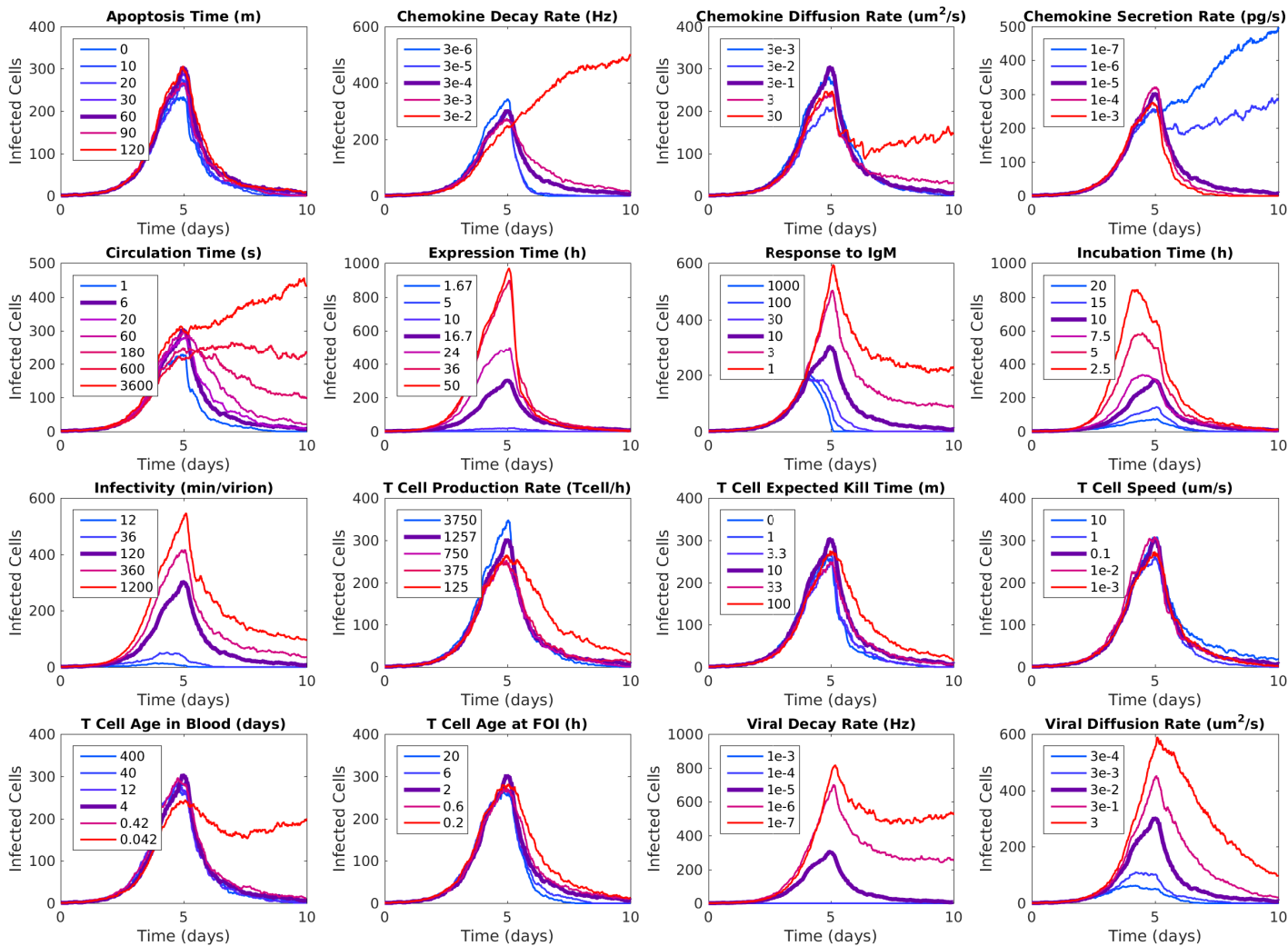


Figure S4. aH5N1 sensitivity analysis. The sensitivity analysis results for 16 parameters applied to the aH5N1 model simulation. In each subplot, the thicker purple line shows the results of the model using the default parameter value.

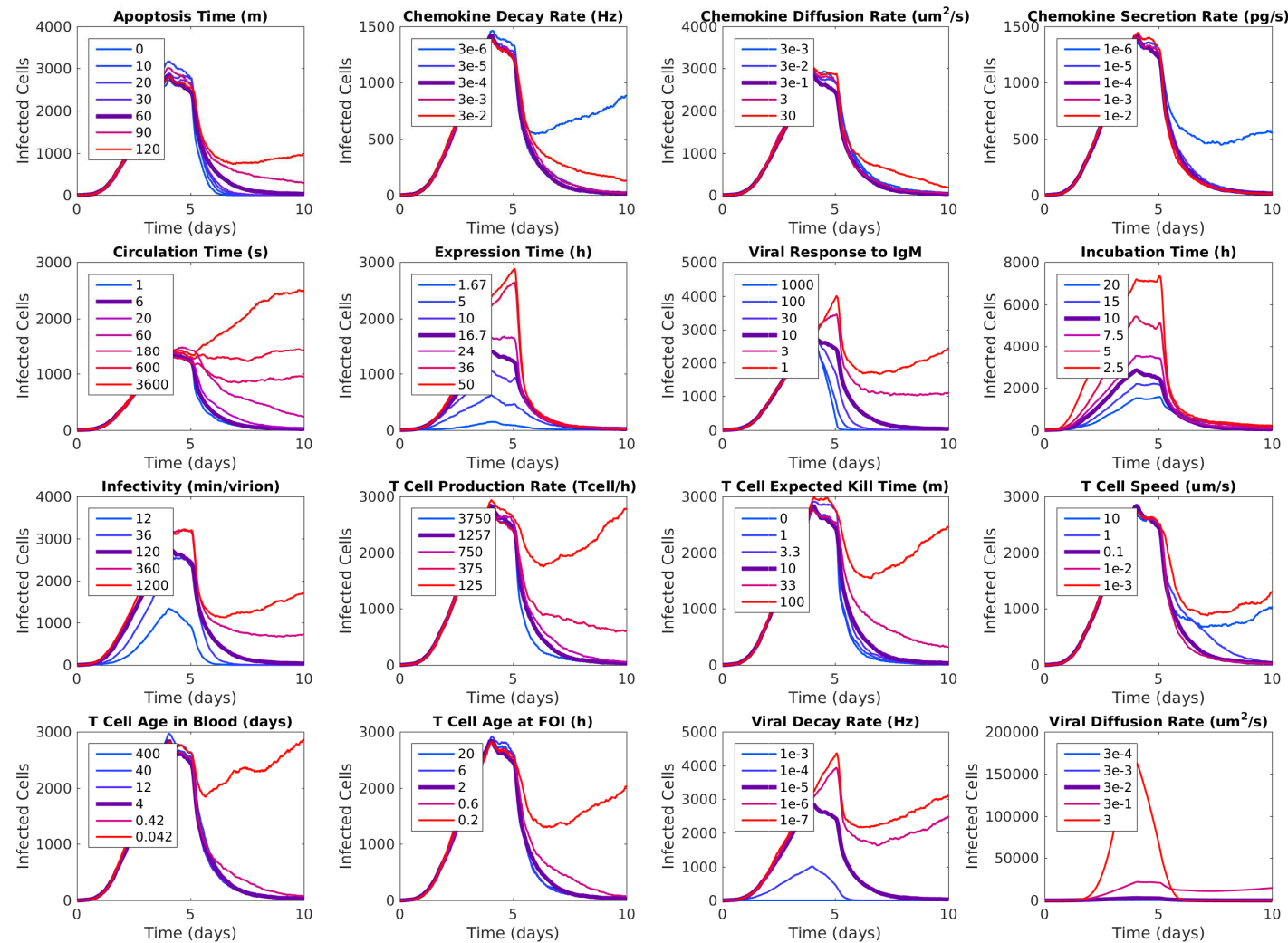


Figure S5. sH1N1 sensitivity analysis. The sensitivity analysis results for 16 parameters applied to the sH1N1 model simulation. In each subplot, the thicker purple line shows the results of the model using the default parameter value. The divergence between Apoptosis Time values of 90m and 120m (upper-left plot) highlights an important threshold of infection control.

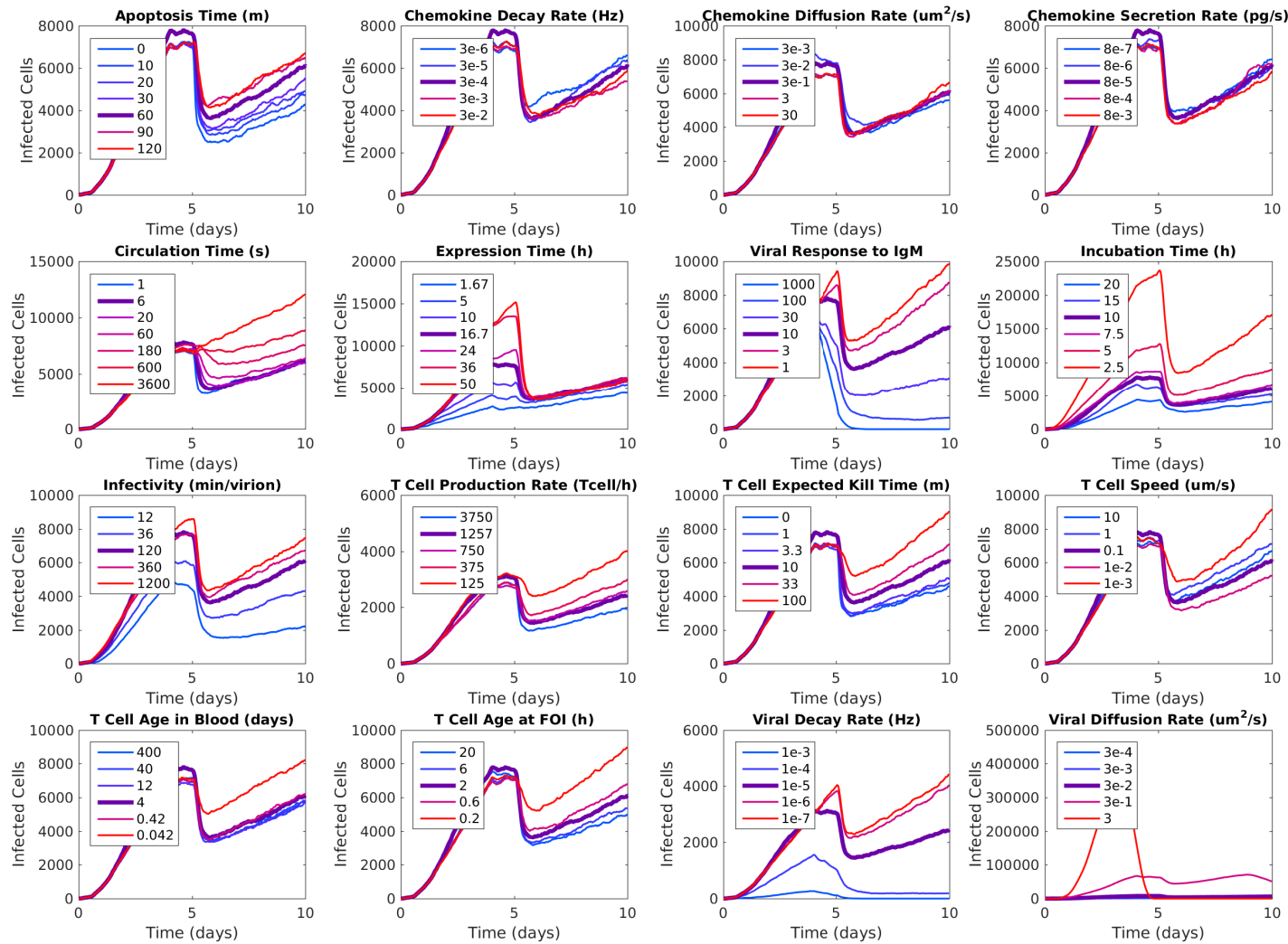


Figure S6. pH1N1 sensitivity analysis. The sensitivity analysis results for 16 parameters applied to the pH1N1 model simulation. In each subplot, the thicker purple line shows the results of the model using the default parameter value.

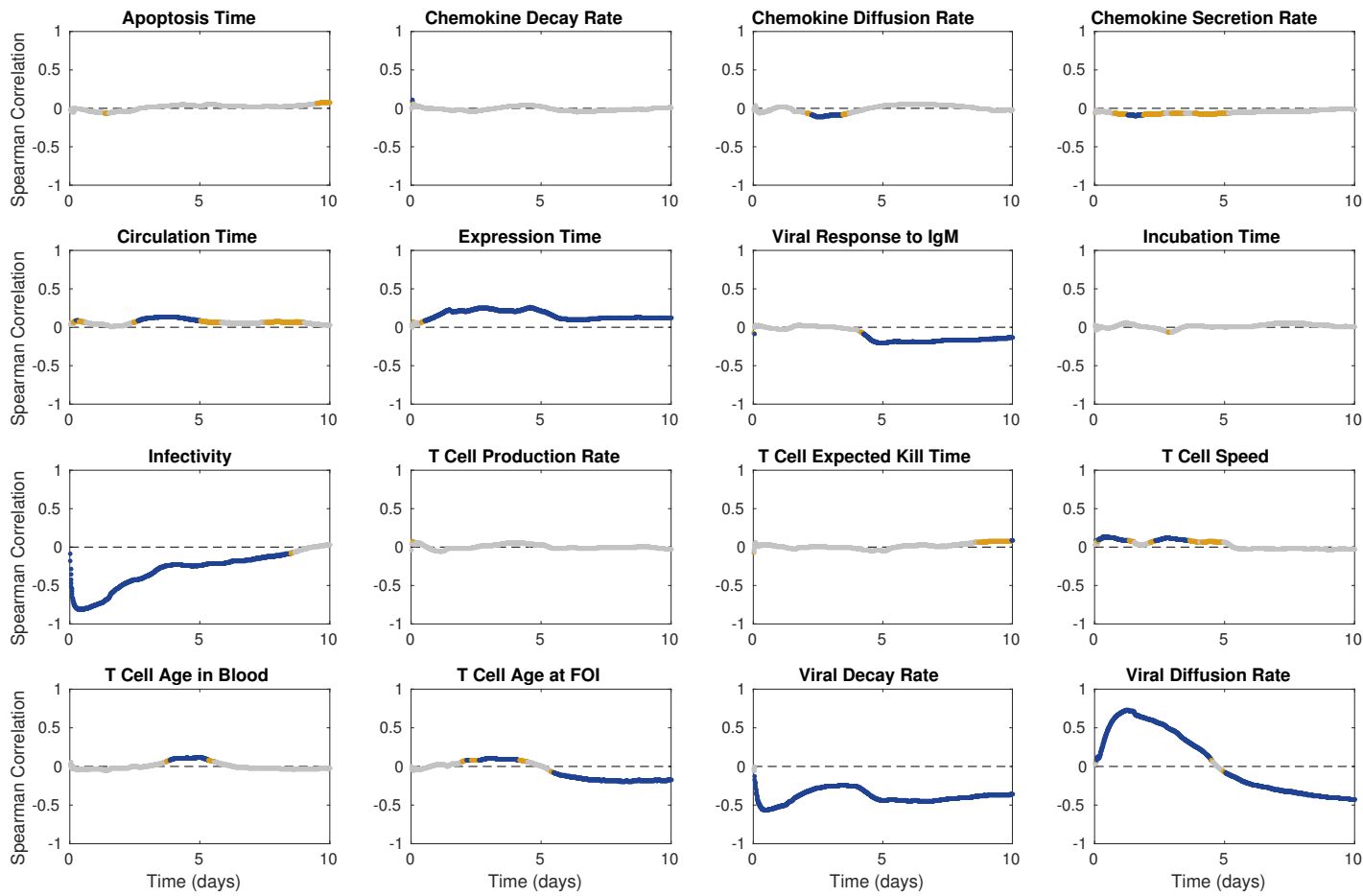


Figure S7. PRCC sensitivity analysis. PRCC analysis generated Spearman correlation coefficients (ρ) and significance values (p) over 1441 time points. Plots show values of ρ vs. time for each parameter tested. Dark blue indicates significance levels at $p < 0.01$. Gold indicates significance of $p < 0.05$. Light gray indicates $p \geq 0.05$. Six parameters show significant effect over the time period where they were relevant to model dynamics: infected cell expression time, viral response to IgM, viral infectivity, T cell expected lifetime at the FOI, viral decay rate, and the viral diffusion rate.

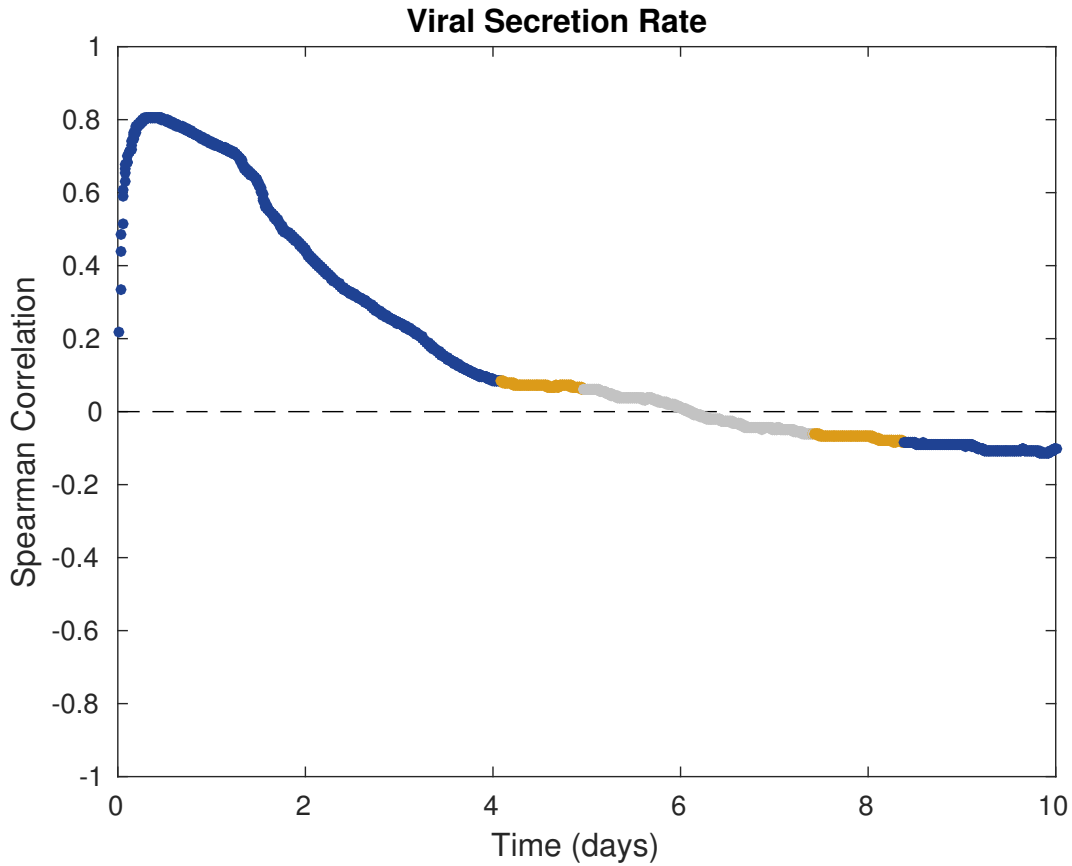


Figure S8. PRCC sensitivity analysis for the viral secretion rate. Similar to Figure S6, PRCC analysis generated Spearman correlation coefficients (ρ) and significance values (p) over 1441 time points. Plot shows the values of ρ vs. time for the viral secretion rate. Dark blue indicates significance levels at $p < 0.01$. Gold indicates significance of $p < 0.05$. Light gray indicates $p \geq 0.05$. Viral secretion shows significant effect on model output. The decline of ρ over time reflects the early death of every modeled target cell (Figure S9).

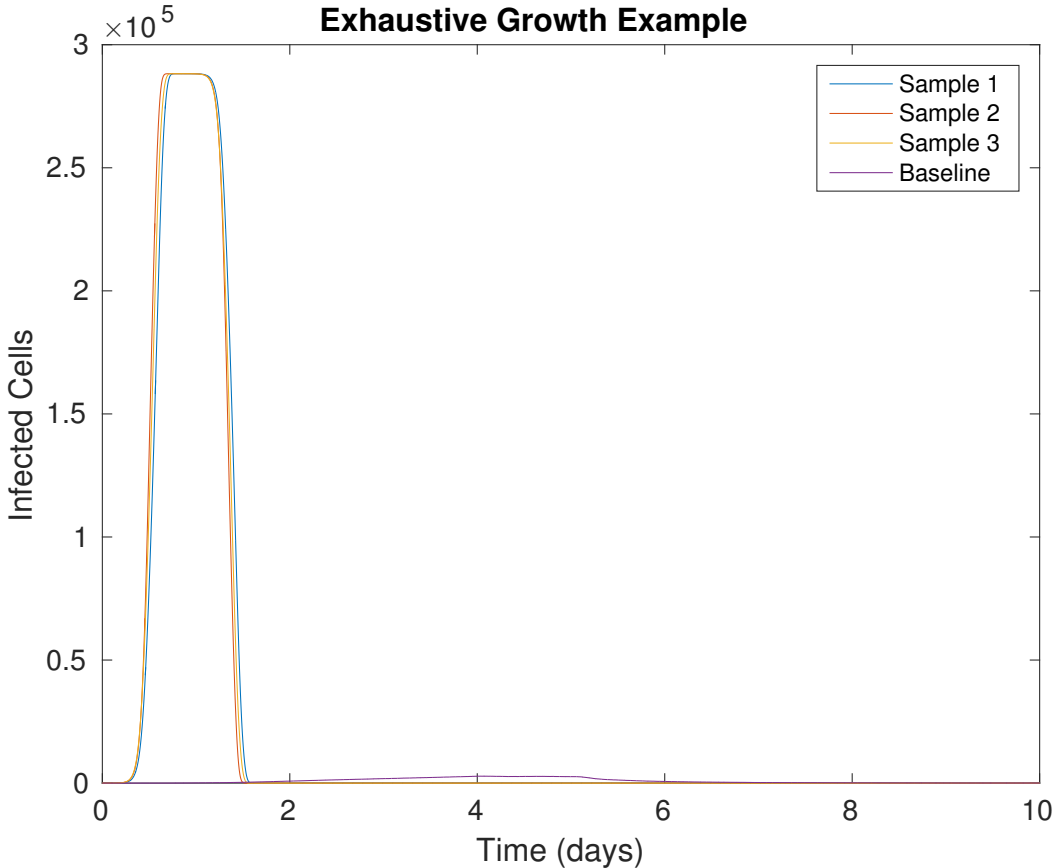


Figure S9. Exhaustive Growth: Certain parameter sets generated by Latin hypercube sampling caused rapid uncontrolled infection growth (Samples 1-3). This resulted in the early death of every modeled target cell (saturation at day 1) and the inevitable decline of the infection size to zero. A larger, unbounded model environment would show unconstrained growth. This effect explains the decline of the ρ value of several viral parameters to or past zero over time in Figures S7 and S8.

Video S1. The first of three overlaid videos of a representative seasonal H1N1 infection. This video spans the 10 day infection and shows the cells as they transition from healthy to infected to dead. T cells show half way through the simulation. Healthy cells are gray, virus-incubating cells are yellow, virus-secreting cells are orange, apoptotic cells are red, and T cells are green.

Video S2. The second of three overlaid videos of a representative seasonal H1N1 infection. This video spans the 10 day infection and shows the virus concentration. Notice the volatility when T cells arrive halfway through the simulation. Virus concentration ranges from $1e-13$ mols/mL (white) to $1e-27$ mols/mL (black). Refer to Figure 5 for the detailed legend.

Video S3. The third of three overlaid videos of a representative seasonal H1N1 infection. This video spans the 10 day infection and shows the chemokine concentration. Notice the volatility when T cells arrive halfway through the simulation. Chemokine concentration ranges from 1e8 ng/mL (white) to 1e-6 ng/mL (black). Refer to Figure 5 for the detailed legend.

Video S4. A closer look at the 2009 pandemic simulation. This video shows the infection from day 6 to day 7 with each frame spanning 1 simulated minute. Healthy cells are gray, virus-incubating cells are yellow, virus-secreting cells are orange, apoptotic cells are red, and T cells are green. Note the high proportion of virus-secreting cells (orange) early on. As time passes, secreting cells are gradually contained to the point where they become very sparse. T cell clumping often prevents the T cells from quick discovery of new secreting cells.

Tables

aH5N1			sH1N1			pH1N1		
Time hours	CXCL10 pg/mL	CCL5 pg/mL	Time hours	CXCL10 pg/mL	CCL5 pg/mL	Time hours	CXCL10 pg/mL	CCL5 pg/mL
0	440	1	0	94	62	0	179	45
2	391	0	2	24	45	12	1,835	55
8	1,723	1	8	87	50	16	1,349	46
12	3,462	1	10	296	57	20	23,458	150
16	4,618	2	16	770	87	24	12,073	93
20	6,807	6	20	3,048	134	32	30,700	380
24	8,164	16	24	3,901	151	48	19,814	1,224
30	> 8,500	68	28	8,261	150			
38	> 8,500	239	32	12,935	245			
48	> 8,500	655	38	26,970	780			
72	> 8,500	415	42	24,120	695			
			72	21,441	1,665			

Table S1. Empirical cytokine titers for three strains of influenza. Measured CXCL10 (IP-10) and CCL5 (RANTES) shown in pg/mL for three strains of influenza: Avian H5N1, Seasonal sH1N1, and Pandemic pH1N1. sH1N1 IP-10 secretion exceeded measurement accuracy above 8500 pg/mL. Human bronchial epithelial cells were infected at an MOI of 0.01 (10,000 virions) with one of the three strains of influenza. Basal media for chemokine secretion was collected at the given time intervals post infection. Chemokine levels were measured using 30 μ L aliquots for a panel of 17 chemokines and cytokines (not shown).

Population	Description	Initial Value
T	Healthy target epithelial cells	1,000,000
I_1	Virus-incubating cells	0
I_2	Virus-secreting cells	0
V	Free virus particles	10,000
F	Interferon quantity	0
C	Chemokine quantity (ng/mL)	0
Parameter	Description	Value
β	Viral infection rates	
	Avian	5.3e-7 (PFU·h) ⁻¹
	Seasonal	6.1e-7 (PFU·h) ⁻¹
	Pandemic	2.7e-6 (PFU·h) ⁻¹
p	Viral production rates	
	Avian	0.20 (PFU/h)
	Seasonal	1.4 (PFU/h)
	Pandemic	18.3 (PFU/h)
e	Interferon strengths	
	Avian	1.0e-8
	Seasonal	1.6e-6
	Pandemic	3.4e-3
τ_2	Interferon production delays	
	Avian	21.5 (h)
	Seasonal	23.6 (h)
	Pandemic	21.0 (h)
δ	Virus-secreting cell decay rate	0.6 (h ⁻¹)
d	Chemokine decay rate	1.386 (h ⁻¹)
τ_1	Viral incubation time	10 (h)
τ_3	Chemokine production delays	
	IP-10	8 (h)
	RANTES	16 (h)

Table S2. Parameters for Preliminary Model 1 (Equation 1). All parameters and populations are taken from (Mitchell et al., 2011) except for C , d , and τ_3 . The value chosen for d corresponds to a 30 minute half-life and values for τ_3 were set from the observed chemokine data (Fig. 3). Interferon (F) is an abstracted unitless quantity and thus e is a unitless multiplier.

Strain	Chemokine	RMSE
aH5N1	RANTES	166
	IP-10	7,950
sH1N1	RANTES	90
	IP-10	2,732
pH1N1	RANTES	2,671
	IP-10	64,342

Table S3. Root mean squared error of Preliminary Model 1 fits. Preliminary Model 1 (Eq. 1) was fit to experimental data (Table S1) using a genetic algorithm as described in the main paper. The resulting model fits can be seen in Figure S1.

Paramter	Value	Source	I	C
T(0)	1e6	(Mitchell et al., 2011)	4	329
V(0)	1e4	(Mitchell et al., 2011)	58	997
r_{cell}	5 μm	(Miao et al., 2010)	816	2550
t_{rc}	6s	(Peters, 1983)	3,264	4,410
k_e	6.4e - 5/cell/day	(Miao et al., 2010)	10,050	8,069
β	4.8e - 7/cell/PFU	(Mitchell et al., 2011)		
p	0.18PFU/h	(Mitchell et al., 2011)		
δ	16.7hours	(Mitchell et al., 2011)		
a	67.7	ABM fits		
b	433.5	ABM fits		

Table S4. Parameters for Preliminary Model 2 (Equation 2). Values are chosen to match the equations borrowed from both (Mitchell et al., 2011) and (Miao et al., 2010). Values a and b were fit to multiple runs of a simplified CyCells ABM using the linear model $C = a\sqrt{I} + b$ with a resulting $R^2 = 0.997$, $P < 0.01$.

Category	Parameter	Units	Distribution
Chemokine	Chemokine Decay Rate	Hz	LN(-3.4, 1.0)
	Chemokine Diffusion Rate	$\mu m^2/s$	LN(-0.5, 1.0)
	Chemokine Secretion Rate	(pg/s · cell)	LN(-3.7, 0.1)
T Cell	Circulation Time	seconds	LN(-.75, 0.5)
	T Cell Kill Rate	min	LN(1.0, 0.5)
	T Cell Speed	$\mu m/min$	LN(-.75, 1),
	T Cell Age in Blood	days	LN(0.6, 1.0)
	T Cell Age at FOI	min	LN(2.1, 0.5)
	T Cell Production Rate	cells/h	LN(3.1, 0.15)
Delay	Apoptosis Time	hours	U(0.0, 2.0)
	Expression Time	min	LN(3.0, 0.15)
	Incubation Time	hours	LN(-1.0, 0.15)
Virus	Viral Response to IgM	—	LN(1.0, 0.5)
	Infectivity	min/virion	LN(2.1, 0.5)
	Viral Decay Rate	day ⁻¹	LN(0, 1.0)
	Viral Diffusion Rate	$\mu m^2/s$	LN(-1.5, 1.0)
	Viral Secretion	(PFU/s · cell)	LN(-3.4, 0.3)

Table S5. Latin hypercube sampling distributions. LHS was used to generate sample points containing each of the 16 parameters from Table 3, plus the sh1N1 viral secretion rate. Parameters were sampled over biologically plausible ranges listed here for use in PRCC analysis. LN signifies a log-normal distribution. Values were sampled from a regular normal distribution with the listed parameters and then transformed to linear space from \log_{10} space. U signifies a uniform distribution.

Strain		Slope (PFU/s)	Intercept (PFU)
Avian H5N1	I(t)	5.86e-8	-0.0133
	D(t)	1.03e-7	-0.0223
Seasonal H1N1	I(t)	3.25e-7	0.0225
	D(t)	6.93e-6	0.0439
Pandemic H1N1	I(t)	8.79e-7	0.093
	D(t)	2.71e-4	5.28
Strain	Avg. $E(t)$	Estimated R_0	
Avian H5N1	0.355	1.16	
Seasonal H1N1	0.049	1.11	
Pandemic H1N1	0.0037	1.12	

Table S6. Linear fits to model runs for $I(t)$ and $D(t)$ across all three strains. Every parameter was significant at the $p < 0.05$ level. $E(t)$ is estimated to be $I(t)/[I(t) + D(t)]$. $E(t)$ does not vary by more than 10% from day 5 to day 10, thus the average of each is calculated and used to estimate R_0 for all three strains in the absence of a T cell response.